

SATURN: A Thin and Flexible Self-powered Microphone Leveraging Triboelectric Nanogenerator

NIVEDITA ARORA*, STEVEN L. ZHANG, FERESHTEH SHAHMIRI, DIEGO OSORIO, YI-CHENG WANG, MOHIT GUPTA, ZHENGJUN WANG, THAD STARNER, ZHONG LIN WANG, and GREGORY D. ABOWD, Georgia Institute of Technology, Atlanta, USA

We demonstrate the design, fabrication, evaluation, and use of a self-powered microphone that is thin, flexible, and easily manufactured. Our technology is referred to as a Self-powered Audio Triboelectric Ultra-thin Rollable Nanogenerator (SATURN) microphone. This acoustic sensor takes advantage of the triboelectric nanogenerator (TENG) to transform vibrations into an electric signal without applying an external power source. The sound quality of the SATURN mic, in terms of acoustic sensitivity, frequency response, and directivity, is affected by a set of design parameters that we explore based on both theoretical simulation and empirical evaluation. The major advantage of this audio material sensor is that it can be manufactured simply and deployed easily to convert every-day objects and physical surfaces into microphones which can sense audio. We explore the space of potential applications for such a material as part of a self-sustainable interactive system.

CCS Concepts: • **Human-centered computing** → **Interaction devices**; • **Hardware** → **Power and energy**; **Communication hardware, interfaces and storage**;

Additional Key Words and Phrases: flexible electronics, passive microphone, Triboelectric effect, TENG (Triboelectric Nanogenerator), applications

ACM Reference Format:

Nivedita Arora, Steven L. Zhang, Fereshteh Shahmiri, Diego Osorio, Yi-Cheng Wang, Mohit Gupta, Zhengjun Wang, Thad Starnier, Zhong Lin Wang, and Gregory D. Abowd. 2018. SATURN: A Thin and Flexible Self-powered Microphone Leveraging Triboelectric Nanogenerator. *Proc. ACM Interact. Mob. Wearable Ubiquitous Technol.* 2, 2, Article 60 (June 2018), 28 pages. <https://doi.org/10.1145/3214263>

1 INTRODUCTION

Sound is a critical source of information for understanding and controlling the environment. Sound is sensed using a microphone, an acoustic–electric transducer, which outputs an electrical signal that reproduces the sound pressure variations that it senses. In addition to the obvious applications of recording events for playback and automated speech recognition, the increased availability of low-cost embedded microphones has resulted in a variety of other interesting applications. These applications include occupancy detection [16, 25], control [30, 45, 56], human behavior studies [4], structural maintenance [15], health monitoring [27, 70], hearing aids [5], activity recognition [26, 40, 63, 80] and sound source localization [48, 62].

*This is the corresponding author

Authors' address: Nivedita Arora, nivedita.arora@gatech.edu; Steven L. Zhang; Fereshteh Shahmiri; Diego Osorio; Yi-Cheng Wang; Mohit Gupta; Zhengjun Wang; Thad Starnier; Zhong Lin Wang; Gregory D. Abowd, Georgia Institute of Technology, Atlanta, USA.

Permission to make digital or hard copies of all or part of this work for personal or classroom use is granted without fee provided that copies are not made or distributed for profit or commercial advantage and that copies bear this notice and the full citation on the first page. Copyrights for components of this work owned by others than ACM must be honored. Abstracting with credit is permitted. To copy otherwise, or republish, to post on servers or to redistribute to lists, requires prior specific permission and/or a fee. Request permissions from permissions@acm.org.

© 2018 Association for Computing Machinery.

2474-9567/2018/6-ART60 \$15.00

<https://doi.org/10.1145/3214263>

Proc. ACM Interact. Mob. Wearable Ubiquitous Technol., Vol. 2, No. 2, Article 60. Publication date: June 2018.

As ubiquitous as microphones may seem today, there is still room for progress. A microphone's design balances several important features, including recording quality, form factor (e.g., size, weight, flexibility, thickness), and power consumption. Electronic devices most commonly use electret [54] or condenser [46] microphones based on MEMS technology [11, 71]. CMOS–MEMS acoustic devices allow miniaturization and on-chip electronics, but are active, that is, they require power for operation and sound amplification [8, 12]. Commercially available passive (or self-powered) microphones do not consume power but are bulky (e.g., a moving coil dynamic microphone [7]) or use PVDF films, which either results in a low sensitivity contact microphone [1, 38] or complex to manufacture and costly to scale in size [24, 53]. The challenge lies in designing a microphone which is passive and has sound quality comparable to its active counterparts (acoustic sensitivity > -25 dB_{SPL}) while still preserving a lightweight and versatile form factor [28]. Recent advances in materials science have demonstrated the possibility of such self-powered, easy-to-manufacture sensors that take advantage of the triboelectric nanogenerator (TENG) to convert mechanical vibrations into electrical energy [65, 67, 69]. The TENG relies on the triboelectrification and electrostatic induction effects, which converts tiny mechanical vibrations into electric signal output without applying an external power. In this paper, we present the design, fabrication, and evaluation of a flexible and self-powered microphone that is made up of a thin and inexpensive PTFE/paper/copper structure.

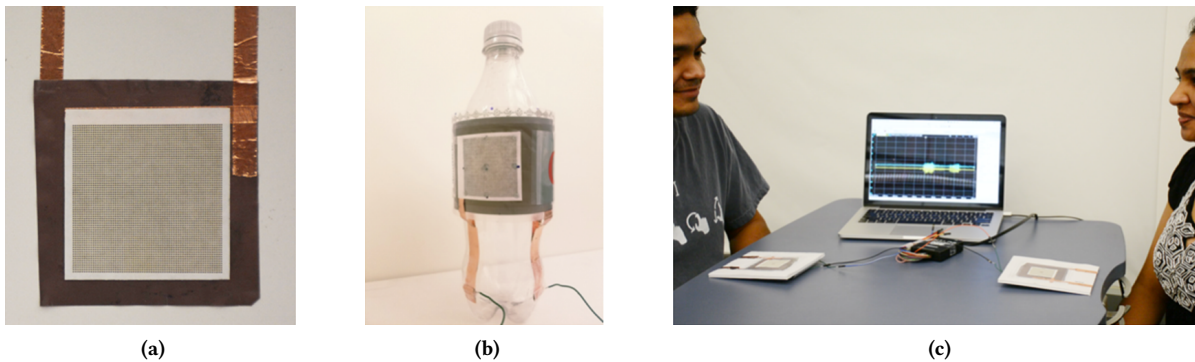


Fig. 1. SATURN Microphone in variety of configurations (a) Close-up of the device (b) Soda bottle with flexible microphone to enable interactions (c) Sensing table to detect location of people around it

Our solution results in a **Self-powered Audio Triboelectric Ultra-thin Rollable Nanogenerator (SATURN)** microphone. This paper provides three research contributions for the SATURN microphone:

- **Device fabrication:** Inspired by the thin, flexible design of a sound energy harvester based on the triboelectric nanogenerator (TENG) [10], we have developed a simpler and cheaper fabrication technique for the SATURN Microphone.
- **Discovering optimal design performance:** Several design parameters impact the performance of the SATURN microphone, specifically the geometry of a SATURN patch, the size and spacing of holes in the paper layer, and the method of attaching the various layers to each other. In this work, an iterative evaluation strategy which balanced empirical results against a theoretical understanding of the device was adopted to guide our design in order to achieve best performance. We built a simulation model of the SATURN material to examine how design parameters affect the propagation of sound vibrations across the material. We also empirically characterized the sound quality (acoustic sensitivity, frequency response, and directivity) in a controlled laboratory setting and offer a comparison against commercially available alternatives. This theoretical–empirical balance gives us confidence that our final design is both reproducible and understandable.

- **Evaluation of interesting usage contexts:** The SATURN microphone provides an advantageous form factor which is thin and flexible and can be exploited in a number of planar and circular configurations. We demonstrate the potential of the SATURN microphone in setting where its flexibility and passivity are best utilized. We compare SATURN microphone's sensitivity to other COTS microphones. We also suggest device system solutions which exploit the self-powering characteristics of the SATURN microphone for loud decibel sound event detection.

Demonstration of SATURN microphone design, fabrication and applications can be found at the following link:

www.youtube.com/watch?v=OLuZHpa_FIM

2 RELATED WORK

The last decade saw significant research efforts towards building low power electronics [22, 36, 47, 59, 61]. In addition to better power management strategies, there has been a recent push to make embedded devices thin and flexible [39, 72]. To achieve this overreaching vision of self-sustainable flexible electronics, materials science and microelectronics communities have been working on new device designs for sensing [43, 52], computing [42], feedback [79], energy harvesting [50] and storage [23] which leverage new materials, nano-structures, and printing technologies. The UbiComp research community has often sought ways to make these technological innovations more practical, reliable and easy to use for various applications [19, 20].

To build low (or no) power and versatile form factor electronics, we need to start from individual device components which follow this trend, so that in the future these components can be assembled together as a single working unit. An example of one such device component is a self-powered sensor. Energy harvesters can be redesigned to have high sensitivity for the phenomenon they generate energy from, to create sensors which do not require power to be operated. A new breed of self-powered sensors based on the triboelectric effect work exactly on this concept, and one recent example is the Triboelectric Nanogenerator (TENG) [64, 65, 67]. The design of these sensors is based on the principles of triboelectrification (or contact electrification) and electrostatic induction and convert any kind of mechanical energy to a highly correlated electrical response. With their lightweight, low-cost, and high efficiency even at low frequency, TENGs have been shown as passive or self-powered sensors for detecting mechanical motion such as pressure[33, 76], touch[6, 17], vibrations[3, 73], linear displacement[34, 78], speed [74], rotation[32], and acceleration[77]. Beyond saving power, TENG-based sensors are flexible, fulfilling the requirements for a sensing unit for skin-like devices. In this paper, we are inspired by the promise of TENGs and demonstrate how a simpler manufacturing process that does not rely on any sophisticated nano manufacturing can be used to develop a self-powered sensor for capturing vibrations from sound.

There have been previous attempts to build triboelectric-based acoustic energy harvesters. Yang et al.[75] designed a resonant air cavity using TENG structure based on aluminum and polyvinylidene fluoride (PVDF) which converted loud sounds (e.g., a clap) to an electrical signal. This approach was redesigned to be flexible by Fan et al. [10] using a PTFE-nanowire and paper-based device structure. As an energy harvester, the experiments were focused on maximizing electrical response at the natural resonant frequency. Thus, only low range frequencies for loud sounds at high sound pressure were tested. Recently, other nano-structure designs based on a ferroelectric nanogenerator (FENG) [31] and piezoelectric nanogenerator (PENG) [68] have also been explored to make flexible acoustic sensors, actuators, and energy harvesters.

The triboelectric effect is not new to researchers wanting to leverage it for interactive purposes. Karagozler et al. used the triboelectric effect to support simple interactions in a children's storybook [19]. Paradiso's Interactive Balloon used the piezoelectric properties of PVDF mounted on a mylar balloon to record sounds [44], demonstrating practical use of a self-sustaining acoustic sensor. These examples, as well as the insights from the above-mentioned materials science work, inspire our development of the SATURN microphone. What sets

the work of this paper apart from all of this previous work is a rigorous exploration of the design features that make triboelectric-based acoustic sensing practical for a variety of interesting application scenarios. These design features include:

- **Low-cost fabrication:** Previous work employs nano-fabrication techniques, like inductive coupling etching-process (ICP etch), microplasma discharge [31], and nanowire growth [10]. These methods must be precise, which makes the device fabrication on a practical manufacturing scale difficult, expensive, and requiring a high skill level for production. We seek a fabrication technique that is inexpensive and does not significantly compromise signal quality.
- **Wider acoustic range:** Low frequency ranges (< 1000 Hz) and high sound pressure levels are sufficient to demonstrate a device as a sound energy harvester, working at some resonant frequency, but not to demonstrate the device as a sound sensor. For example, in telephony, the usable frequency band range for voice is approximately 300 Hz to 3400 Hz. We seek a flexible thin sound sensing material which is sensitive across this wider band of the human audible range. We also want sensitivity beyond the voice band, including up 4-6 kHz for sound clarity and definition.
- **Performance reliability:** Fabrication techniques should be reproducible i.e two microphones produced with the same technique should be similar in acoustic performance.

Our paper hopes to bridge the gap between material science and ubiquitous computing communities for self-powered, flexible acoustic sensors. We explore a simpler fabrication technique for the SATURN microphone versus the techniques for the original TENG devices. We provide a detailed and reproducible guide to construct SATURN microphones which can be followed, and improved upon, by others. We evaluate the SATURN microphone's audio characteristics and compare it with state-of-the-art microphones. In Section 9, we demonstrate two implemented applications of the SATURN microphone to show its use in practice. Those implemented applications, however, only exhibit the passive microphone capabilities of SATURN and still require traditional powered components to receive and process the audio signal.

3 HOW THE SATURN MICROPHONE WORKS

3.1 Theory of Operation : Triboelectric Nanogenerator

The operation of the SATURN microphone is based on the principle of two, coupled phenomena—electrostatic induction and contact electrification. Electrostatic induction is the generation of opposite charges on two different materials, while contact electrification or triboelectrification, is charge transfer between two surfaces in contact. The fundamental theory of triboelectrification lies in Maxwell's displacement current and change in surface polarization [66]. By introducing a thin conducting electrification layer, the charge difference between the two polarized surfaces generated due to triboelectricity can be measured. This combined structure is called the triboelectric nanogenerator (TENG). The polarity and strength of the charges produced are dependent on many material variables such as surface roughness, temperature, and dielectric constant.

3.2 Device Design

The multi-layered device structure of the SATURN microphone is schematically depicted in Figure 2. It consists of a thin film of dielectric polytetrafluoroethylene (PTFE), which has a permanent negative charge stored on its surface, sandwiched between two copper layers. These copper layers act as electrification layers that generate triboelectric charges upon coming in contact with PTFE. The first layer of the copper is laminated on the PTFE itself (bottom layer) while the other is deposited on paper (top layer). The paper in the SATURN microphone structure is neutral and used only for structural support for the copper electrification layer which comes in contact with PTFE due to vibration. To minimize the air friction which dampens the vibrations, holes have been introduced on the paper to act as a mini-resonant cavity for air when sound propagates, resulting in enhancement

of the vibration effect. Paper is used because of its flexibility, lightweight structure, low cost, and ease of cutting holes.

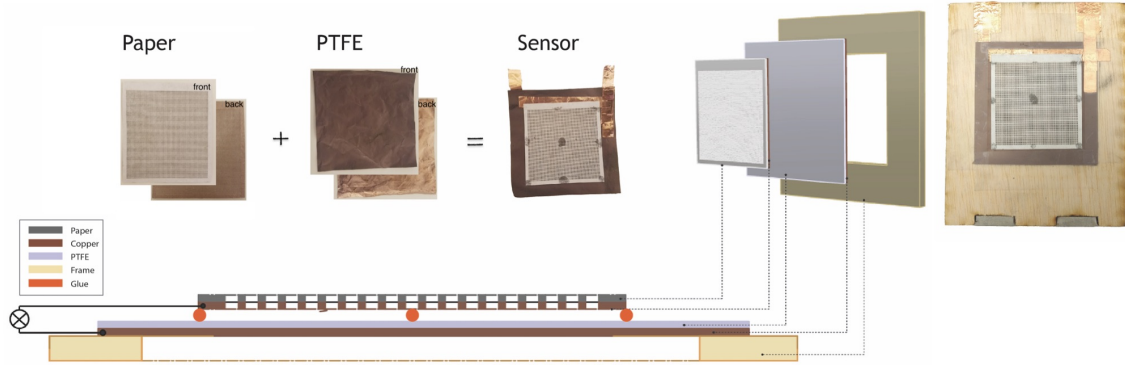


Fig. 2. Structural design of SATURN Microphone consisting of copper coated paper and PTFE

3.3 Working Mechanism

The SATURN microphone works on the principle of vibration-induced contact and charge generation due to triboelectrification and electrostatic induction. This process is explained in detail in Figure 3. Propagation of the sound through air causes compression and rarefaction corresponding to the frequencies present in it.

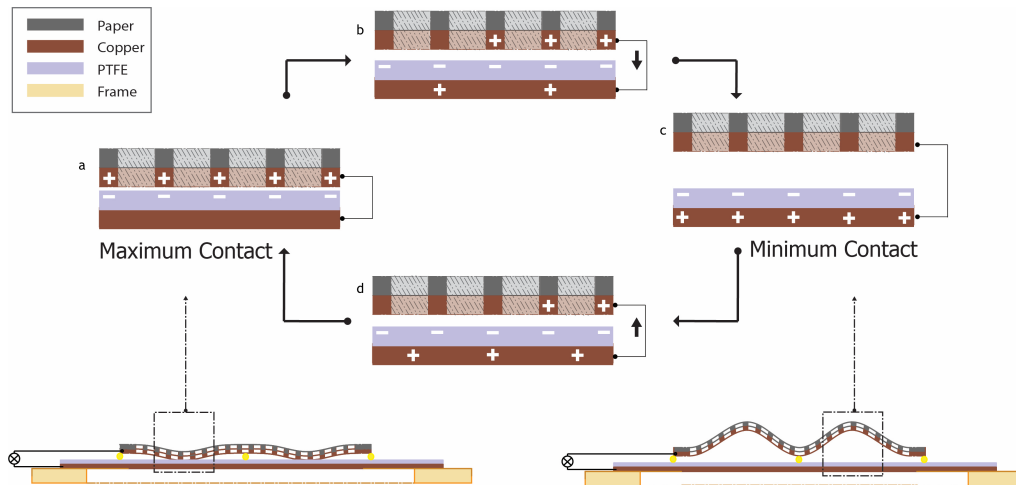


Fig. 3. Cycle of electricity generation process under external acoustic excitation

When a compression is incident on the SATURN microphone it causes vibrations in its membrane-like structure, resulting in the copper layer on the paper coming in contact with the PTFE (Figure 3 a). Contact electrification generates charges on both surfaces—PTFE, which has a greater electron affinity, is able to gain electrons from the copper[2] and becomes negatively charged, whereas the copper layer on the paper becomes positively charged. When subsequent rarefaction separates the paper and the PTFE (Figure 3b), it induces a potential difference across the two copper electrodes, causing current to flow from paper towards PTFE if the device is connected to

an external load. This flow of current reverses the polarity (Figure 3c) of charges on the two copper electrodes (i.e., now the copper on PTFE has more positive charge than the copper layer on the paper). The next compression results in the paper moving towards the PTFE again, resulting in a reversed direction of current flow (Figure 3d), completing the cycle of electricity generation.

4 FABRICATION

The SATURN microphone consists of two attached layers—paper and PTFE, both with a deposition of copper (Figure 4). The fabrication steps are explained in detail below and depicted in Figure 4.¹

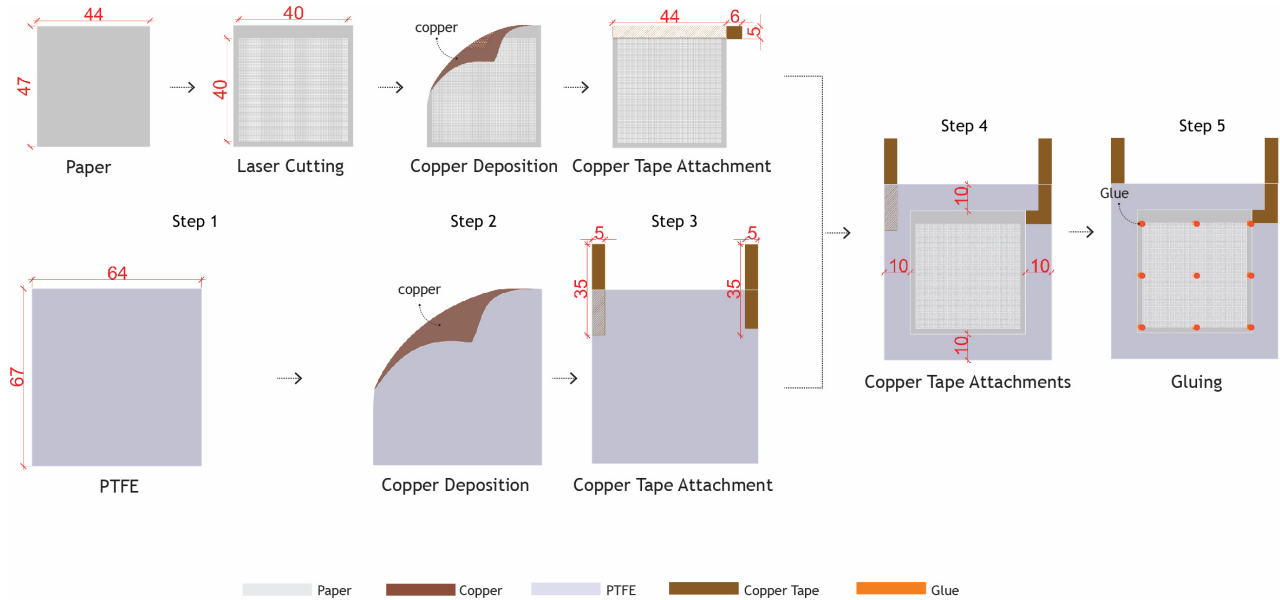


Fig. 4. Fabrication Process : (1) Preparation of micro-hole paper (2) Deposition of copper layer (3) Attaching copper tape as electrodes (4) Stacking paper and PTFE (5) Gluing paper and PTFE. All dimensions are in mm.

- (1) **Preparation of micro-hole paper** : We start with standard copier paper of 0.04 mm thickness. 400 μm diameter holes with an even spacing of 200 μm are cut into the paper in a grid pattern using a micro-laser cutter, a Universal Laser System PLS6MW using 9.3 μm CO_2 at 80% power and a 700 PPI raster mode at 20% speed. The hole pattern forms a 4cm x 4cm square grid. A small border of 5mm on one side and 2mm on the other side is left to be used for attachment to the PTFE layer. This border is kept small to ensure ease of reproducibility of the cavity created between copper and paper after being attached together.
- (2) **Deposition of copper layer** : The paper sheet with micro-holes (step 1) and a PTFE sheet (6cm x 6cm with 0.05 mm thickness) are coated on one side with a thin layer of copper that act as electrodes. The copper is applied using a standard sputtering technique inside a PVD chamber (a Leskar PVD75) with a chamber pressure of 6×10^{-6} torr. The deposition time is set to 45 minutes, resulting in a 0.15 μm copper layer thickness on the paper and the PTFE. This allows the copper to deposit on the paper but not obstruct the micro-holes. The border of the perforated-paper is also coated with copper.

¹Video of fabrication process: www.youtube.com/watch?v=ITJPWALCYe8

- (3) **Attaching copper tape as electrodes** : We attach conductive copper tape to the copper coated side of the paper and the PTFE in order to extend the electrodes for measurement purposes or to connect to an external circuit.
- (4) **Stacking paper and PTFE** : The paper and PTFE are placed on top of each other such that the copper layer of paper is on top of the non-coated side of PTFE, which is non-conducting. To avoid a short circuit, we ensure that the copper tape attached to the copper coated side of the paper does not touch the copper laminated side of the PTFE and vice versa. Finally, the copper tape from the paper is attached to the second copper tape on the uncoated side of PTFE.
- (5) **Gluing paper and PTFE** : The paper layer (copper side facing PTFE) is glued to the uncoated PTFE side using glue dots at nine anchor points.

Structural parameter values mentioned above, like hole size, hole spacing, and attachment points for paper to PTFE, were determined by performing experiments and simulation, as discussed in detail in Section 5 on device design optimization. The final thickness of the constructed SATURN microphone patch is measured to be $150 \mu\text{m}$, which is comparable to that of standard copier paper. This sensor can be attached to objects using glue on the edges of copper side of the PTFE layer.

5 DEVICE DESIGN OPTIMIZATION

The main aim of device design optimization for SATURN microphone is to increase electrical response across wider range of frequencies in order to achieve a better acoustic sensitivity. This allows sounds of lower decibel levels to be detected, thus opening doors for wide variety of applications.

5.1 Factors Effecting Device Performance

The SATURN microphone consists of paper and PTFE, which are both flexible and vibrate to act as two plates of a capacitor to produce an electrical response. In previous descriptions of the behavior of a Triboelectric Nanogenerator ([65, 66]), it was assumed that the two layers are rigid. In that case, the open circuit potential difference generated by the device as a function of time(t) is given by the equation [41]:

$$V_{oc} = \frac{\sigma x(t)}{\epsilon_0} \quad (1)$$

where, $x(t)$ is the physical separation distance between the PTFE and paper, σ is the charge density generated on the surface, and ϵ_0 is the relative permittivity of the dielectric. This mathematical model is overly simplified, and would not work for SATURN microphone because neither the paper nor the PTFE layer are rigid. In practice, the PTFE layer will be attached to a surface, so we will continue to assume it is rigid. The paper layer, however, behaves more like a flexible membrane and will vibrate. Keeping the vibration of paper in mind we have derived a modified formula below.

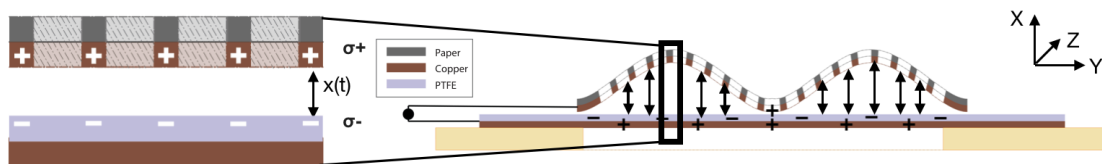


Fig. 5. Factors effecting potential difference generation : $\sigma_{effective}$ surface charge density and $d_{effective}$ separation distance between the two plates

The separation distance between the paper and PTFE layers changes over time when we assume that the paper layer is vibrating, as shown in Figure 5. When our membrane is placed in the Y-Z plane of a right-handed reference coordinate frame, if we take an infinitesimal element with area $dy \cdot dz$ at a location $(0, y, z)$ w.r.t. the origin, then the potential difference across the infinitesimal element is a slight modification of equation 1 and is given by:

$$V_{oc} = \frac{\sigma_{eff}}{\epsilon_0} x(y, z, t), \quad (2)$$

where σ_{eff} is the effective surface charge density, and the separation distance x is a function of y , z and time, which varies along y and z for the flexible membrane. Hence, the open circuit potential difference for a flexible paper layer can be written as:

$$V_{oc} = \frac{\sigma_{eff}}{A\epsilon_0} \iint_A x(y, z, t) dy dz. \quad (3)$$

To increase V_{OC} for the SATURN microphone there are two parts in this equation which can be optimized:

- (1) σ_{eff} : Effective surface charge density which is dependent on the roughness of the PTFE surface; and
- (2) d_{eff} : Effective separation distance during flexural vibrations is $\iint_A x(y, z, t) dy dz/A$ and is mainly dependent on the ability of the paper to vibrate.

5.2 Method of Evaluation

To guide our structural device design we use combination of two evaluation techniques:

- (1) **Simulation** : a structural modal analysis to simulate the dynamic vibration behavior of the paper in order to determine d_{eff} , amplitude of effective separation distance; and
- (2) **Experiment** : an empirical experimentation with fabricated SATURN microphones to determine the electrical response in a controlled sound environment

5.2.1 Structural Modal Analysis. Modal analysis is the method to identify the natural frequencies of vibrations of a material and the mode shapes of a structure. The deformed shape of the structure at a specific natural frequency of vibration is termed as its mode shape of vibration. A thin membrane-like structure such as that of SATURN microphone has infinite modal frequencies and mode shapes. The material response for a given input load is linear combination of these mode shapes. We used a 3-D finite element (FE) model mesh using tetrahedral elements to perform the modal analysis using ANSYS.² The glued attachments points of the paper with PTFE (described in Step 5 of the fabrication process in Figure 4), were meshed separately, to be assigned as fixed support (see Figure 6a).

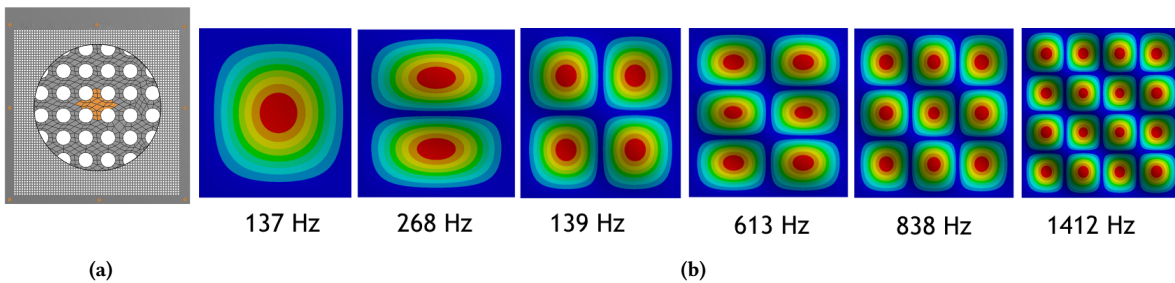


Fig. 6. Modal analysis done using ANSYS Inc. software : (a) 3D Finite Element model of paper with meshed tetrahedral structure with zoomed in central fixed support point. (b) Modal shapes of paper at different natural frequencies.

²<http://www.ansys.com/>

We use lower modes of vibrations, i.e., mode shapes with lower natural frequencies, as they are easy to visualize with the number of peaks and crests less as compared to the mode associated with a higher natural frequency. Figure 6b shows an example of different modes of vibration for paper anchored around the edges.³ The transverse deformation, or vertical deflection, is plotted with the help of colored contours. For each normal mode shape, the contours are plotted and arranged from blue to red such that blue represents zero or negligible vertical deflection whereas red represents the location of maximum vertical deflection possible.

The value of the vertical deflection of a point, obtained from the modal analysis, is referred to as the amplitude of separation of a point, $x(y,z,t)$ in Equation 3. The integral of the amplitude of separation at each of these points is d_{eff} or $\iint_A x(y, z, t) dy dz/A$. We will choose the structural design which has a higher d_{eff} during modal analysis, as it will have a higher electrical response. For structural designs which have the same boundary condition (points of fixation) we can also use d_{max} , maximum amplitude of separation of the same mode shape to compare. This is because calculating d_{max} is simpler than determining d_{eff} which involves integral.

5.2.2 Acoustic Characterization : Sensitivity and Frequency Response. We use frequency sweep, or chirp as the input sound recording to observe the electrical response of SATURN microphone to characterize its quality. Chirp is a sine wave linearly increasing in frequency (20Hz-20kHz) in a particular time period (Figure 7). We standardize the 1000 Hz frequency to sound pressure level of 94 dB_{SPL} or 1 Pa pressure. The power in dB re mV/Pa at 1000 Hz frequency is defined as acoustic sensitivity of microphone. It is used as a representative of the sound quality of a microphone. JBL Flip 2 speaker (100 Hz-20kHz flat frequency response) is used as sound input device (frequency sweep, tone) for our experiments. The sound loudness was measured using Sound Pressure Level (SPL) meter by Extech Instruments. The electrical response generated by SATURN microphone is measured as voltage using Analog Discovery oscilloscope which has 1 M Ω resistance.

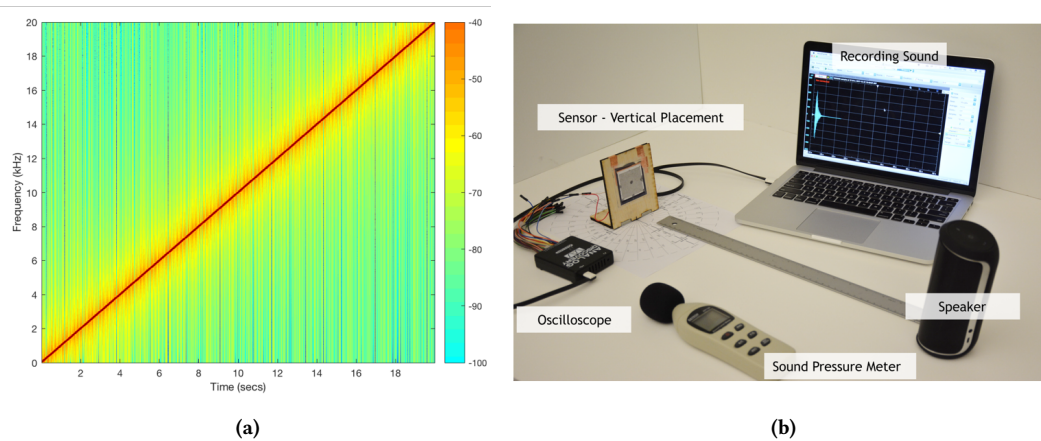


Fig. 7. Acoustic Characterization: (a) Chirp sound Input : linearly increasing 20Hz-20000 Hz frequency sweep in 20 seconds (b) Experimental setup for recording electrical response of SATURN microphone.

Figure 8 shows an example of the electrical response for SATURN microphone for the chirp sound input. We use voltage as a measure of the electrical response, as the current produced by the SATURN device is extremely small (nano-amps in magnitude), which makes it susceptible to the background noise. The maximum voltage is achieved at the resonant frequency of approximately 275 Hz. At 1000 Hz, the acoustic sensitivity is -26.63 dB re

³We used values of 3 GPa Young's modulus of elasticity, 0.04 mm thickness, 47mm x 44mm dimensions, and 1.2 g/cm^3 density for the vibrating paper layer.

mV/Pa. We will be using both a frequency response curve and acoustic sensitivity to select optimal structural design parameters.

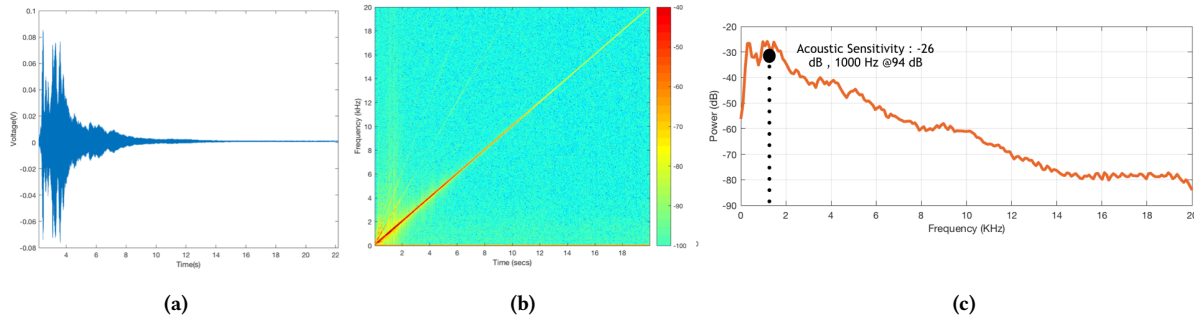


Fig. 8. Example of electrical response from SATURN Microphone for chirp sound input: (a) Voltage time series output (b) Spectrogram with linearly increasing frequency (c) Acoustic sensitivity variation across the audio frequency band (20Hz-20kHz).

5.3 Separation Distance Optimization

The paper layer is a critical component to be designed precisely in the SATURN microphone structure to maximize the separation distance between the two layers and hence the output from the device. To do so, we introduce various structural changes to the paper layer, described next.

5.3.1 Pattern of Holes in the Paper Layer.

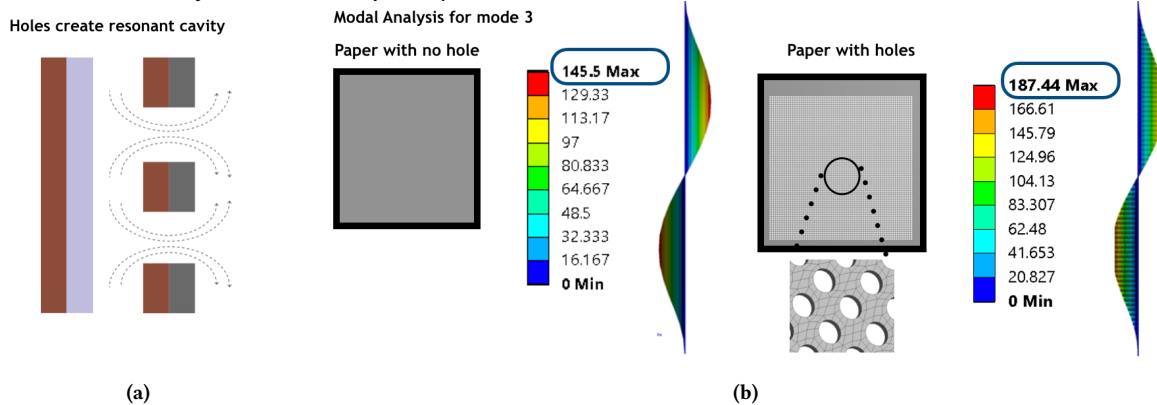


Fig. 9. Introduction of holes enhances vibration: (a) mini-resonant air cavities formed between paper and PTFE which result in reduction of air-dampening (b) Example of modal analysis of paper with and without holes showing introduction of holes increases the d_{max} and d_{eff}

The introduction of holes in a structure is a well known techniques to enhance vibrations in it. To test this hypothesis, we performed modal analysis of a sheet of paper (3 GPa Young's modulus of elasticity, 0.04 mm thickness, 47mm x 44mm dimensions) and compared it with perforated paper with holes (400 μ m diameter, 200 μ m spacing) (Figure 9). Both the models have similar mode shapes due to similar rigid support points and material properties. This allows for comparison on the basis of two parameters, both of which are representative of the voltage response V_{oc} :

- d_{max} : The magnitude of maximum transverse deformation of paper with no holes is $145 \mu\text{m}$, as shown in the legend in Figure 9, while paper with no holes is $187 \mu\text{m}$ which is approximately $40 \mu\text{m}$ less.
- d_{eff} : Paper with no holes has effective separation distance of $40 \mu\text{m}$, while the one with holes is $45.3 \mu\text{m}$.

Both parameters d_{max} and d_{eff} , suggest that the holes on the paper can help in the optimization of separation distance. We can explain this by the following reasons:

- Holes allow the air to flow between the two layers, allowing air to pass through the holes and force the two layers to move away from each other.
- Perforated paper has less stiffness. Bending stiffness of a structure refers to the resistance to transverse deformation. Thus, the perforated paper layer would result in larger separation distance as compared to the paper layer without holes.

While introducing holes increases the separation between layers, it also reduces the contact surface area and thus effective charge density σ is decreased, which would decrease the voltage. Thus, there is a trade-off between contact area and the hole parameters of size, distribution, and pattern. Modeling vibrations of the system to respect air pressure changes and weight is beyond the scope of this paper. Instead, we provide empirical results to determine good hole dimensions.

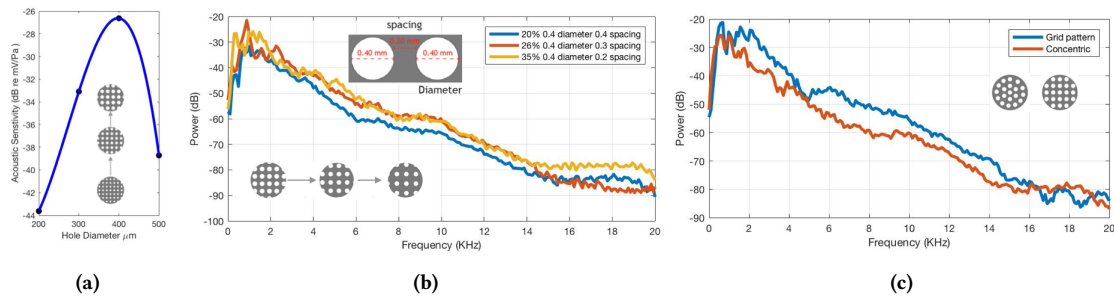


Fig. 10. Selection of dimensions for hole on paper: (a) 0.4 mm diameter hole had the best acoustic sensitivity amongst different diameter sizes we tested. (b) Frequency response for different hole spacing shows that 0.2 mm spacing performs the best with 0.4mm diameter. (c) Circular and grid hole pattern performance.

Keeping the distance between holes fixed at 0.2 mm, we fabricated a $4 \times 4 \text{ cm}^2$ SATURN microphone patches with increasing hole diameter (Figure 10). 0.4 mm diameter hole achieved the best acoustic sensitivity of -26 dB among our samples. Next keeping the hole diameter at 0.4 mm we increased the spacing between the holes to be 0.2 mm, 0.3 mm, and 0.4 mm i.e having percentage of hole area to be 35%, 26%, and 20% respectively. SATURN microphone with 0.3 mm spacing gives the best acoustic sensitivity but the device with 0.2 mm spacing performs slightly better within the first 2 kHz frequency band, where more than 70% of the sound information is present[9]. Next, we experimented with two different patterns of holes – concentric and grid – to determine their effect on the frequency response. The grid pattern of holes performed better than concentric pattern arrangement We determined previously in our hole distribution study that 35% hole area performs better than the 25% hole area. Since grid has 35% hole area it performs better than the concentric circle which is 25%. Thus, for all our future experiments and modal analysis we will choose to use 0.2 mm hole spacing, 0.4 mm hole diameter in a grid pattern.

5.3.2 Paper and PTFE Attachment Position. By controlling the locations where paper is attached to the PTFE in the SATURN microphone structure, we can generate motion with a higher amplitude of motion with the same sound input. This can be done by choosing attachment points which are coincident with the nodes of zero

movement for majority of the mode shapes possible (Figure 11). We tested two cases for the perforated paper model: glued across all the edges; and glued at 9 points like a grid.

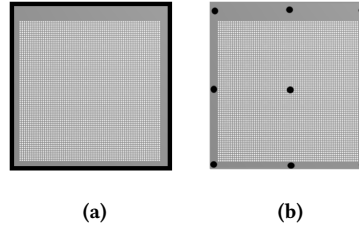


Fig. 11. Different attachment positions: (a) paper glued to PTFE across all edges (b) paper glued to PTFE at 9 points

Figure 12 shows the modal shapes for mode 3 for paper in the two cases discussed. Just by visual observation we can notice that mode shape for paper pasted at edges (case 1) is out of phase, creating minimum and maximum contact with PTFE at the same time, whereas for the 9 glue points (case 2) they are in phase. In addition, as shown the legend, d_{max} for case 2 is $7\mu\text{m}$ ($194\mu\text{m} - 187\mu\text{m}$) more than case 1. This trend is also supported by d_{eff} as case 2 ($52.6\mu\text{m}$) is $8\mu\text{m}$ more than case 1 ($45.3\mu\text{m}$). By simulations we can conclude that 9 points glue grid has more separation distance and thus consequently should generate more electrical signal.

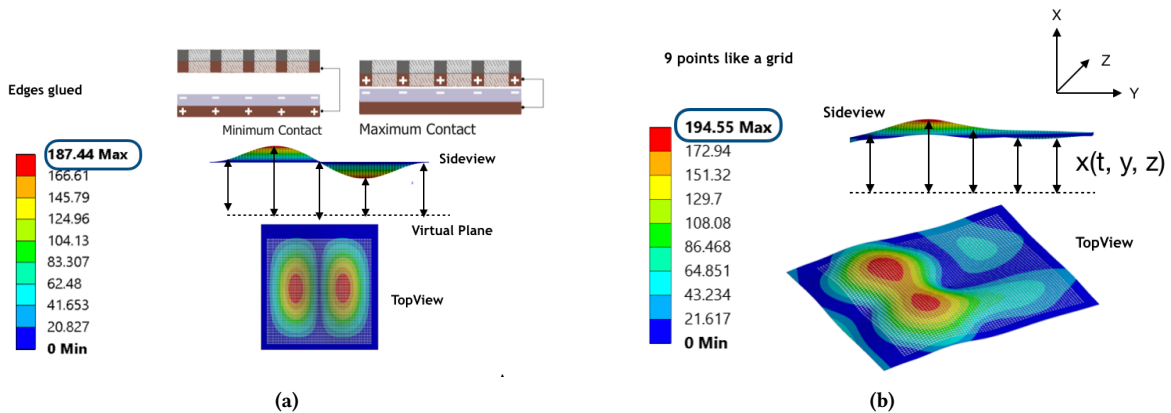


Fig. 12. Modal analysis demonstrates that grid-glye pattern attachment performs better than glue on all edges: (a) mode 3 of paper glued at all edges showing maximum separation distance to be $187\mu\text{m}$ (b) mode 3 of paper glued at 9 points like a grid with maximum separation distance of $194\mu\text{m}$.

We validated these simulation results with empirical measurements. By simply changing the anchoring of the paper layer to the PTFE, there is a large jump of approx 20 dB (re mV/Pa) in the power of the voltage measured (Figure 13a) all across the frequency band.

Having grid like glue pattern allows the edges to vibrate which are otherwise restricted in the glue pattern where all edges are pasted. This effect becomes more enhanced at higher frequencies (mode 14 shown in Figure 13b), where edges have even higher amplitude of separation than even the central nodes. By choosing appropriate boundary conditions of the fixed points, the maximum vibration amplitude can be obtained under certain load conditions to increase the voltage.

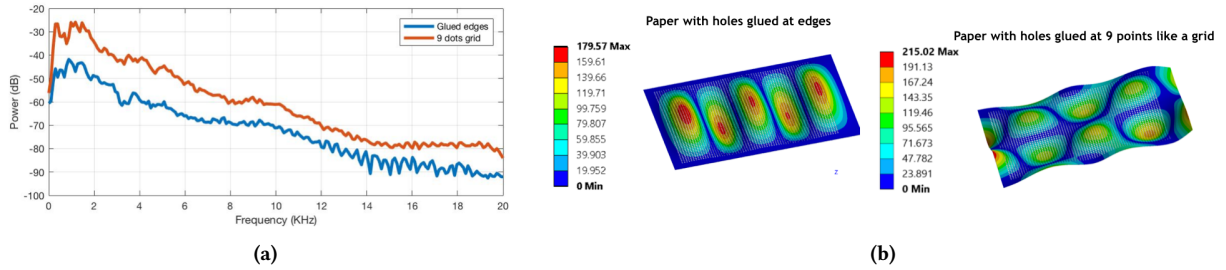


Fig. 13. Impact of gluing pattern: (a) Increase of approximately 20 dB with 9-point grid glue pattern (red line). (b) Modal analysis of perforated square paper with holes pasted at 9 points demonstrating involvement of edges which increases the voltage response.

5.3.3 Changing the Geometry. Changing the geometry of the surface on which sound is incident while maintaining the same area changes the air pressure which is applied at different points. This changes the mode shapes and affects the way the structure will exchange kinetic-energy and strain-energy at its nodes and anti-nodes. Thus geometry impacts the amplitude of vibrations which directly impacts the separation distance and the output voltage.

We tested two different geometries with same 1600 mm^2 area: a square ($4 \times 4 \text{ cm}^2$); and a circle (22.57mm diameter). Experimentally, up to 1000 Hz the circle and square perform nearly the same. For higher frequencies, the circle performs almost 10 dB better than the square (Figure 14a). Thus, choosing a circular shape for the SATURN microphone would improve sound quality. A modal analysis confirms our empirical results. Just by visual inspection the d_{max} , the amplitude of maximum separation reached by circle is almost $16 \mu\text{m}$ more (Figure 14b) than square. We use Equation 3 to calculate d_{eff} , effective separation amplitude, which was found to be $67.2 \mu\text{m}$ for the circle and $52.6 \mu\text{m}$ for the square, that is approximately $15 \mu\text{m}$ more. After optimizing device structural parameters both theoretically and empirically for the separation distance, we are able to reach the best acoustic sensitivity of -25.63 dB (re mV/Pa) at 1000 Hz with a circular shape of 16 cm^2 area with a grid pattern of holes of 0.4mm diameter and 0.2mm spacing glued at 8 equally distant points around the edges and the center to the PTFE.

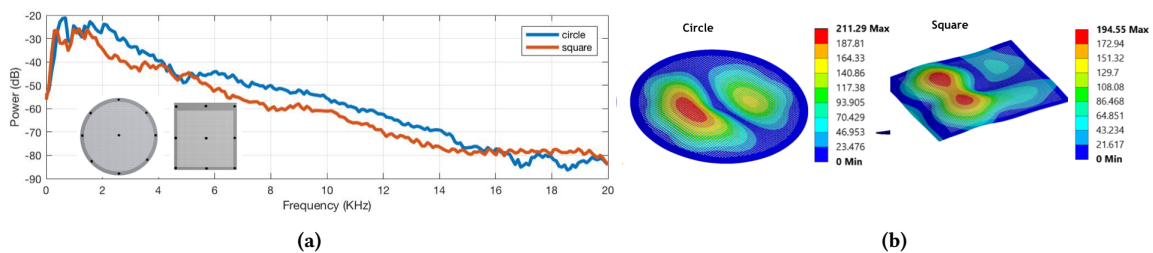


Fig. 14. Circular shape performs better than square of the same area : (a) Experimental analysis of effect of geometry on Frequency response (b) modal analysis for circle and square for mode 3 showing circle has more max. amplitude of separation

5.4 Optimization of Surface Charge Density

5.4.1 Plasma treatment for PTFE surface. Equation 3 shows that the voltage response of the SATURN microphone is dependent on the surface charge density, which is the measure of electric charge per unit length. Fan et al. [10] used PTFE polymer nanowires to increase the charge density σ by increasing the effective surface area of

the dielectric surface in contact. Growing nano-wires is a very expensive process which is currently unsuitable for large scale, low-cost manufacturing. To understand the effect of such nano-structures on PTFE for SATURN microphone's performance, we use a simpler, though still relatively expensive, method called plasma treatment.

The PTFE was etched by O_2 plasma produced by a PE-100 Plasma System (from Plasma Etch Inc.) O_2 was uniformly distributed in the reactor throughout the etching process. Figure 15a shows schematic diagram of the O_2 etching process where a blast of high-speed stream of glow discharge is shot at PTFE. The RF power input was 300 W using a 13.56 MHz RF generator with RF auto-matching network and the plasma treatment time was 20 min. Figure 15b shows the scanning electron microscope (SEM) image of PTFE after plasma treatment. This PTFE was later coated with copper using as general fabrication process explained in section 4. Due to increased roughness on the PTFE surface resulting in increased contact electrification the performance with plasma treatment improves by approximately 10 dB across the entire frequency response as shown in Figure 15c.

Even though there is an increase in the signal quality, with acoustic sensitivity of -16.28 dB re mV/Pa, the cost addition does may not justify the performance increase for SATURN microphone fabrication in many scenarios. Therefore for our further experiments we have tried to focus more on regular PTFE rather than one treated with plasma.

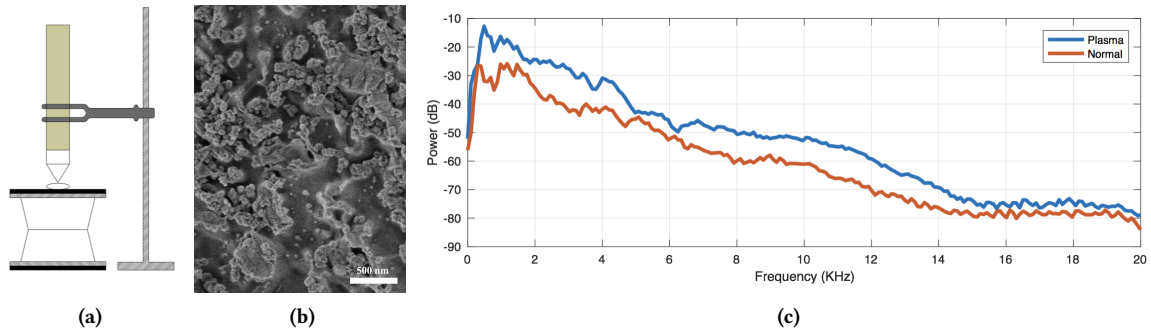


Fig. 15. Effect of Plasma treatment on SATURN microphone sensitivity (a) Schematic diagram of O_2 plasma etching (b) Scanning Electron Microscope (SEM) image of plasma treated PTFE used for SATURN mic manufactured at 500nm scale (c) Experimental comparison between performance of SATURN microphone fabricated with PTFE treated with and without plasma

5.5 Intra-device Performance Results

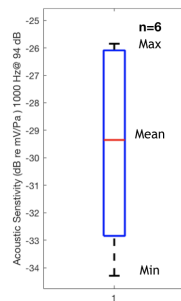


Fig. 16. Intra-device performance of SATURN microphone patch represented as deviation in acoustic sensitivity. (n=6)

To use the SATURN microphone in applications, it is important to have an understanding of the variation in its electrical performance between instances of similarly manufactured examples, what we call intra-device performance. In an ideal device fabrication process, each device should be identical to another, but in practice deviations may be introduced due to different batches of base materials or construction precision. To understand reproducibility of our fabrication process, we constructed six SATURN microphone devices (square $4 \times 4 \text{ cm}^2$ patches, non-plasma PTFE, optimal holes, grid-like glue attachment).

Figure 16 shows the standard deviation of acoustic sensitivity (1000 Hz tone at 94 dB_{SPL}) performance. All devices have $> -35 \text{ dB}$ acoustic sensitivity, with the best performance at -26.44 dB and mean as -29.5 dB . The intra-device reproducibility has tolerance of 10 dB for our fabrication process.

6 MOUNTING OF SATURN MICROPHONE

Just as a pattern of holes allows for greater vibration of the paper layer, so to can the support structure used to mount the PTFE layer affect its vibration, and thus the electrical response of the SATURN microphone.

6.1 Supported vs Unsupported Back Frame Structures

To understand the effect of a back support, we experimented with two kinds of frames (Figure 17a): a full solid back support; and a hollow frame, in which we cut a hole to allow more vibration. The material used for the frame was foam board to which a non-plasma treated $4 \times 4 \text{ cm}^2$ SATURN patch with optimal separation distance parameters was attached.

The performance decreased by approximately 10 dB with the solid back support as compared to the frame with no support. This is because having a support at the back restricts the free movement of PTFE (Figure 17b). Interestingly, having back support showed an increase in sensitivity around $6\text{-}8 \text{ kHz}$, while its framed counterpart just has a decreasing trend. We studied this further by doing modal analysis combined system of of PTFE (440 MPa Young's modulus of elasticity, 0.05 mm thickness, 2.2 g/cm^3 density) pasted to foam-board (Young's modulus 0.1 GPa , 0.5 mm thickness, 0.3 g/cm^3 density). The d_{eff} , amplitude of effective separation for natural frequencies of the system at 2887 Hz is 28 mm while 6900 Hz is about 34 mm . This behavior may be attributed to the coherence of natural frequency of movement for PTFE and back-support. Further consideration of different solid back supports is warranted, as they might produce sensitivity peaks at different frequency bands. We address this next.

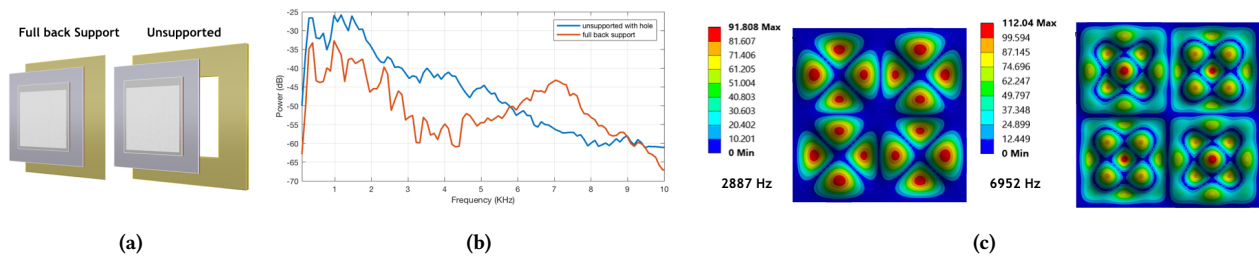


Fig. 17. Effect of different support structures on the signal quality : (a) Frames with full back support and unsupported with hole (b) Frequency response comparison between supported and unsupported (c) Modal analysis of combined PTFE/Foam structure with full back support at 2887 Hz and 6962 Hz which explains the sudden rise in sensitivity around $6\text{-}8 \text{ kHz}$

6.2 Back Support Materials

Even though the framed, unsupported structure is better, there might be situations when a SATURN microphone needs to be embedded directly onto an object. We embedded the device on different material surfaces (Figure 18) to determined their frequency response. Table 1 shows the acoustic sensitivity we recorded from the experiment

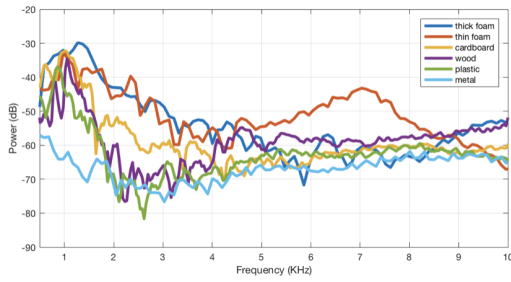


Fig. 18. Frequency response for different frame materials for full back support

Back Support Material	Young's Modulus (GPa)	Sensitivity(dB)
thin foam core	0.1	-30
thick foam board	0.5	-32
cardboard	0.9	-32
wood	3	-35
plastic	10	-37
aluminum	70	-64

Table 1. Effect of back support material on Acoustic Sensitivity of SATURN : Back support material with lower Young's Modulus results in higher sensitivity

versus the Young's modulus of the material. There is a correlation between the flexibility of the material and the sensitivity of a SATURN microphone mounted on that material. For example, metal, with highest stiffness amongst all materials tested, reduces the vibration more than plastic or wood. Thus the back support material properties are a factor in determining the signal quality.

6.3 Orientation

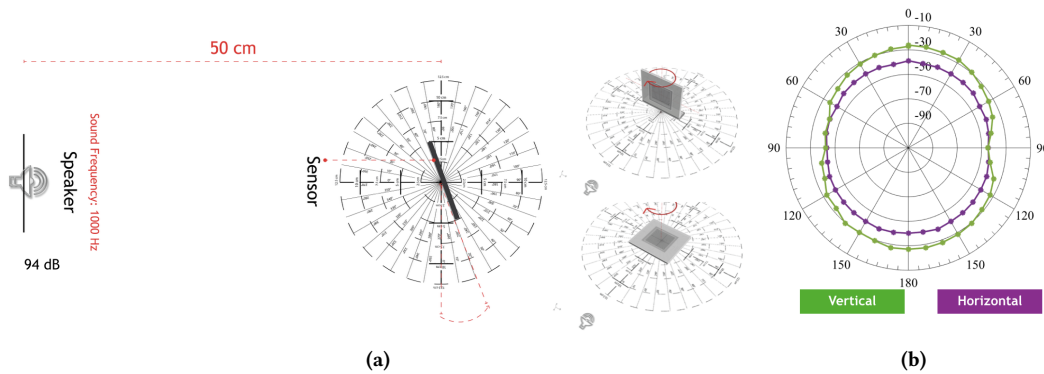


Fig. 19. Effect on orientation on acoustic sensitivity (a) Schematic diagram of experimental setup showing the SATURN microphone in vertical and horizontal positions with 94 dB sound incident (b) polar patterns representing SATURN Microphones' directionality

Changing the orientation of the SATURN microphone changes the sound field incident on it and consequently electrical response produced due to the vibrations. For example, a SATURN microphone placed on a table would receive different amplitudes of voltage for its horizontal and vertical orientations.

To understand this better, we performed an experiment with SATURN microphone ($4 \times 4 \text{ cm}^2$ optimal structural parameters, non-plasma PTFE, attached to foam-board frame with unsupported back) placed horizontally and vertically as shown in Figure 19. A sound source of 1000 Hz frequency tone at 1 Pa was rotated from 0 to 360 degrees around the microphone to plot the directivity pattern. The SATURN microphone is omnidirectional in both horizontal and vertical orientations which is useful for applications such as gathering context in the environment. However, when SATURN is embedded on objects with full back support, we would obtain unidirectional directivity of the microphone, i.e, a semi circle instead of a circle.

In addition when tested for different orientation, there is drop in acoustic sensitivity by 10 dB when SATURN is placed horizontally in front of the sound source as opposed to vertically. Even though vertical orientation is

preferred, there may be applications where horizontal placement is required, as such the experimental comparison is important.

6.4 Patch Size

For a traditional microphone, the size of the diaphragm affects the microphone's sound pressure level handling, sensitivity, dynamic range and internal noise level. The SATURN microphone is similar to the diaphragm of the traditional microphone, so it is reasonable to consider how its size impacts performance.

We did a preliminary test of 3 different sized SATURN patches ($8 \times 8 \text{ cm}^2$, $4 \times 4 \text{ cm}^2$, $2 \times 2 \text{ cm}^2$), each using the structural parameters that produce the best results for the $4 \times 4 \text{ cm}^2$ patch described earlier (Section 5) and placed on vertical frame with sound chirp input. The acoustic sensitivity is -18 dB , -25 dB , and -40 dB respectively, suggesting improved performance for a larger SATURN microphone. These preliminary results show a favorable trend, but a more in depth analysis is needed, and each patch size should be separately optimized, in the same way we optimized for the $4 \times 4 \text{ cm}^2$ size.

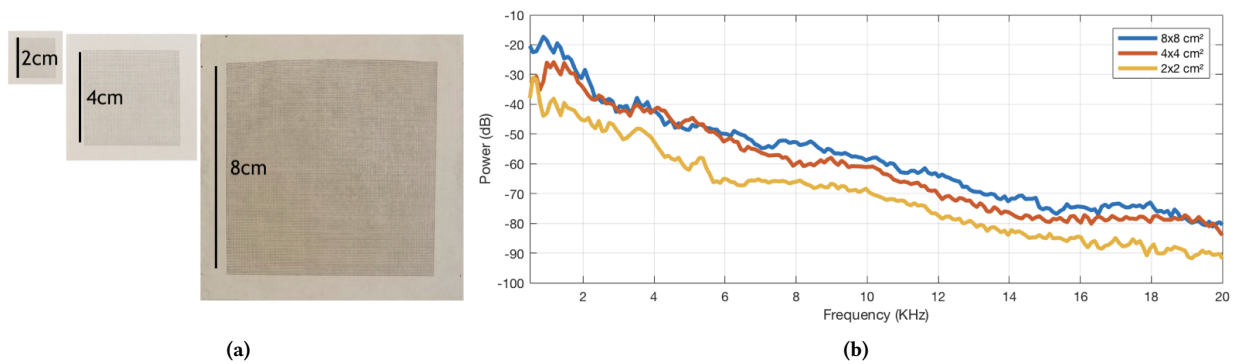


Fig. 20. Effect of SATURN microphone size on the signal quality (a)different patch sizes used for experiment (b) Acoustic sensitivity comparison plot for different sizes

6.5 Flexibility

The SATURN microphone has a thin structure which gives it the affordance to be bent. It is important to understand how the bending impacts the signal quality. Bending of any object adds strain in the object, which leads to increased potential energy, and loss of ability to vibrate or gain kinetic energy. We study the effect of bending using $4 \times 4 \text{ cm}^2$ SATURN microphone patch with non-plasma PTFE with optimal holes size and fixing point. The patch is bent to 7 different radii of curvature corresponding to the central angle theta (5° , 15° , 30° , 45° , 60° , 75° , 100°) as shown in Figure 21a. We performed modal analysis for the curved 3D models of paper with holes for 4 different angles - 5° , 15° , 30° and 45° . Figure 21b shows the effective amplitude of separation, d_{eff} of the 4 models for mode nearest to 1000 Hz, the frequency where acoustic sensitivity is defined. Figure 21c is the snapshot of the corresponding to d_{eff} . We can see that the with increase in bending d_{eff} reduces almost linearly.

Next, we performed the experiment to determine change in acoustic sensitivity with increased bending for fabricated $4 \times 4 \text{ cm}^2$ patch. The SATURN patch was embedded in cardboard as shown in the Figure 22a and bent at 7 different radii of curvature successively making sure that the cardboard follows the lines of curvature. Figure 22b shows successive drop in acoustic sensitivity with smaller radii of curvature, thus following the expected trend from modal analyses. Having a SATURN microphone structure and bending it results in an increased bending stiffness, which effects the ability of the SATURN microphone to vibrate and reduces the voltage it can

achieve. A flat SATURN mic patch used can achieve sensitivity of -27.3 dB which reduces by 8 dB for 45 degrees bent. For the next 45 degrees of bending the drop is much more enhanced as the stiffness increases.

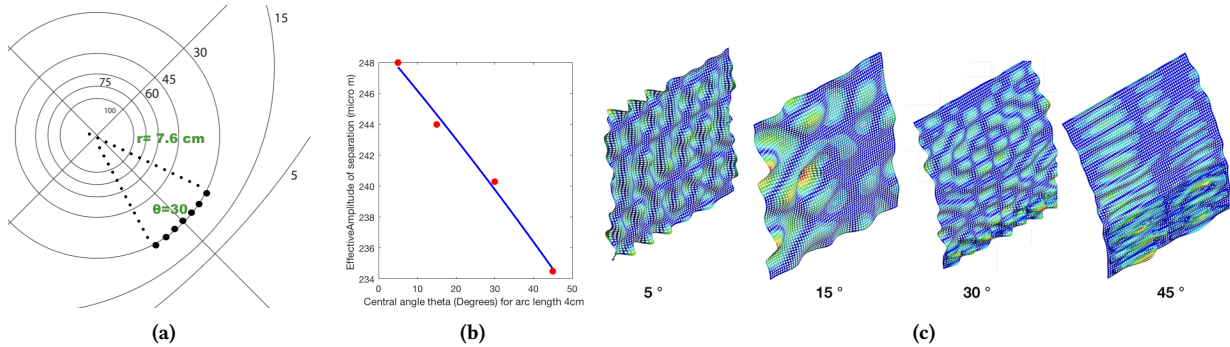


Fig. 21. Effect of flexibility on Effective separation (a) 7 different radii of curvature were drawn on paper corresponding to central angle theta which $4 \times 4 \text{ cm}^2$ patch would make when bent (b) plot demonstrating decrease in effective separation distance with increased bending (c) Modal analysis of 3D meshed model of paper at when subjected to 1 Pa pressure at 1000 Hz

As a result of the design and the fabrication process, the SATURN patch reliability in flexible scenarios may be strongly affected by material stress on the glue points, and tension in the material when transitioning from flat to bended layouts. Some scenarios were tested during the flexibility analysis, however a more extensive analysis on the fabrication process for flexible scenarios is required in order to find a solution that preserve the sound sensitivity and adaptability to different shapes.

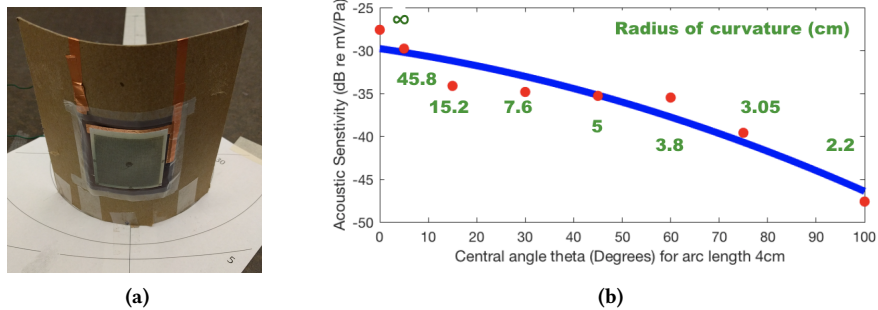


Fig. 22. Experimental results for effect of flexibility (a) SATURN microphone was bent accurately to follow the curved curvature line e.g. 30° (b) Change in acoustic sensitivity (1000Hz @ 94 dB_{SPL}) obtained for different radii of curvature

7 COMPARISON TO COTS MICROPHONE

There are factors in microphone device design—signal quality, power, form factor (size and flexibility) and cost/ease of manufacture—which dictate whether a given acoustic sensor meets the requirements of any given acoustic application. Device designers often face the trade-off between the sensor signal quality and the other design parameters. For example, condenser microphones are used in the recording studio have very high sound quality but consume power in tens or hundreds of mW and are relatively expensive, all of which is appropriate for that niche application. Electret microphones, commonly found in consumer electronic devices, consume

200-500 μW to achieve sensitivity greater than -25 dB. They mostly use power as biasing voltage for the MOSFET or for amplification.

We compared 3 commercially-available off the shelf (COTS) microphones with SATURN mic – 1. iPhone 6s which has invensense INMP441 [18] 2. Sparkfun’s MEMS ADMP 401 with 1.5V of DC bias voltage [58] 3. Omni-Directional Foil Electret Microphone with 1.5 DC bias [57], in the same lab setting with same input chirp sound input as used for our previous SATURN mic experiments. We first performed these experiment in a quiet room with 45dB_{SPL} measured as silence. The SNR was calculated by subtracting the power of the ambient/silent recordings (noise) of the microphone being studied from the power obtained by the chirp input (signal). Since all measurements were done in the same room settings, it is fair to do a comparative measurement of different microphones.

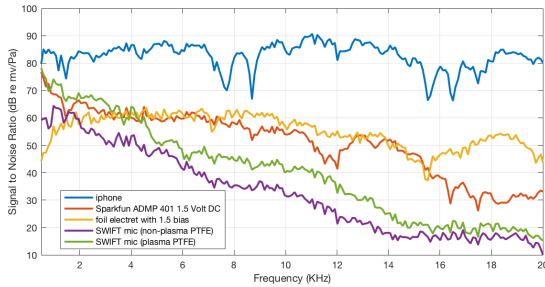


Fig. 23. SNR Comparison with COTS Mic

Mic	1kHz	5kHz	Power(μW)
SATURN plasma	74	60	0
SATURN non-plasma	64.3	50	0
MEMS ADMP-401	67	62	375
Foil electret condenser	58	63	750
iPhone(INMP441)	82	86	2880+

Table 2. SNR(dB) at 1kHz, 5kHz and Power consumed for different mic

Figure 23 shows the Signal-to-noise-ratio(SNR) plot wrt to frequency and the table 2 provides the summary of SNR at 1 kHz and 5 kHz as well as power required by each microphone for operation. At 1000 Hz iPhone’s microphone performed 20 dB better than the non plasma-treated PTFE SATURN microphone and approximately 10 dB better than the plasma-treated PTFE SATURN microphone. This was expected given the iPhone microphone has both hardware and software amplifiers to improve the quality of signal. The SNR curve of the self-powered SATURN microphone with plasma treatment is comparable to Sparkfun ADMP 401 and Foil electret condenser with 1.5 V bias, up to 5000 kHz. The passive SATURN microphone is competitive with some active microphones in terms of signal quality till 5000 Hz. In addition to being self-powered, SATURN microphone’s flexibility lends it the ease of being embedded in different physical objects.

A MEMS microphone is another interesting comparison point. These are also small microphones that can be embedded in objects. They offer low power consumption [29] of approximately $40 \mu\text{W}$ at -20 dB sensitivity. While this may seem like a small power budget, it would not be appropriate for scenarios requiring a large number of microphones or very long life. It would be better to use that power budget for other local computing tasks[13] or communication[61]. MEMS is also a fairly complex micro-fabrication techniques compared to our SATURN design.

8 POWER HARVESTING ANALYSIS

We performed an experiment to determine the peak voltage and peak power of the SATURN microphone as functions of the external load resistance at its resonance frequency. The resonant frequency of the SATURN microphone can vary slightly with each fabricated patch. Thus, we first perform a frequency sweep to determine the system’s maximum $V_{\text{open-circuit}}$ of 0.9 Volts at 255 Hz with a $105 \text{dB}_{\text{SPL}}$ sound source. The measurements for the experiment were done using a capacitive oscilloscope (Kiethley 6514). Next, the external loads were changed successively using a variable resistance box (Elenco electronics) and the corresponding $V_{\text{peak-peak}}$ was

recorded. As shown in Figure 24a, the output $V_{peak-peak}$ increases quickly as the resistance increases from 0.1 Ω to 2 M Ω and approaches an asymptote at 8 M Ω resistance. When we wish to use the SATURN microphone as a sensor, a load resistance of 8 M Ω would give the best result. Such high resistance, however, is not ideal for general electronic circuits. We suggest using a load resistance of 2 M Ω when connecting the SATURN mic as an audio sensor. Figure 24b shows the power vs load resistance curve, where power is calculated as V_{pp}^2/R_{load} . A maximum power of 6.9 micro Watt can be generated from the SATURN microphone at a load impedance of 0.9 M Ω when excited by a 255 Hz tone at 105 dB $_{SPL}$.

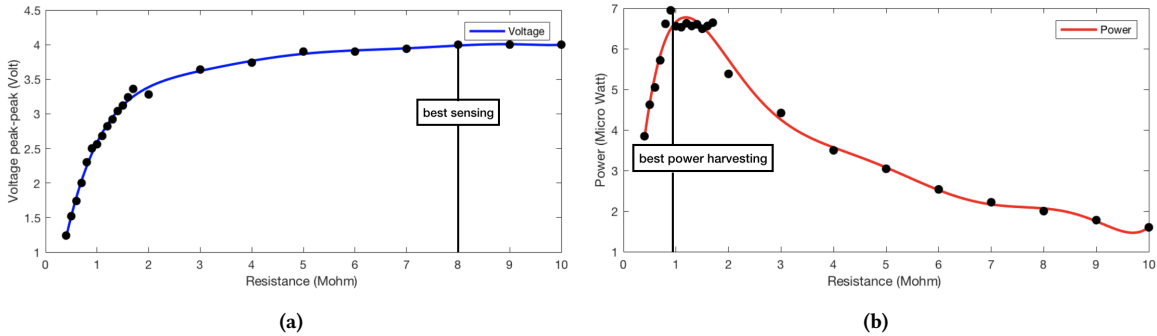


Fig. 24. Determination of load resistance : (a) peak voltage (b) peak power of $4 \times 4 \text{ cm}^2$ SATURN microphone as functions of the external load resistance at resonance frequency

Going further, we analyzed the $4 \times 4 \text{ cm}^2$ SATURN non-plasma microphone patch as a power harvester. The power curve and V_{pp} with a load of 0.9 M Ω at different frequencies is shown in Figure 25. The voltage is approximately 0.5 V $_{pp}$ at 150 Hz and rises to 2.5 V $_{pp}$ and then comes back down again at 350 Hz. The same behavior is shown in the power curve, with a maximum of 6499 nW.

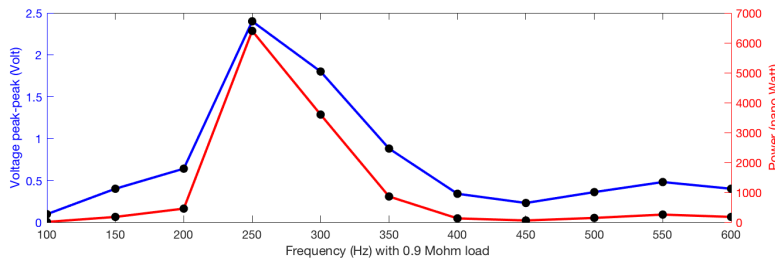


Fig. 25. SATURN as power harvester : Voltage and power generated for different working frequencies

Size of patch	$4 \times 4 \text{ cm}^2$
Type of patch	Non-plasma
Resonant Frequency	255Hz
Load Impedance	0.9M Ω
Max. V_{pp}	2.5V
Max. Power	6944 nW

Table 3. Summary table of power generated by SATURN at 105 dB $_{SPL}$

9 EXPLORING THE APPLICATION SPACE

We explore different application scenarios where the SATURN microphone can be embedded in everyday settings. The applications mentioned are exploratory in nature, and are shown to demonstrate that the quality of the audio signal recovered by SATURN microphone in different configurations is good enough to support a variety of interesting situations. The first two applications take advantage of SATURN as a passive microphone with a thin and flexible form factor. However, the full application still requires signal acquisition and processing

from traditional computing devices. The third example, while not implemented, demonstrates the potential for using SATURN and its power harvesting capability to provide a more end-to-end service.

9.1 Localization of Speakers around a Tabletop

The SATURN microphone is a skin-like sensor that can be placed on different flat or curved surfaces in a room like a curtain, wall, or a table top to gather context. Multiple SATURN microphone patches can easily be placed on the surface of a table, and in combination can be used to localize a speaker. As people speak, the location can simply be determined by comparing voltage output of multiple SATURN microphone patches. The patch placed near to the speaker will pick up more signal than one placed further such that even a simple algorithm of threshold amplitude comparison can detect which speaker is actively talking. Figure 26 shows a simple example of such localization. When speaker A (yellow) speaks, the closer SATURN microphone (1) has higher amplitude than the other microphone (2). Similarly, when speaker B (blue) starts speaking, the closer microphone (2) has higher amplitude than the other microphone (1). Such infrastructure can be expanded to multiple parts of the table, given the number of speakers. We could even imagine placing the SATURN microphones on the walls/ceilings/floors in order to localize speakers within the entire room using more sophisticated processing of the combined signals.

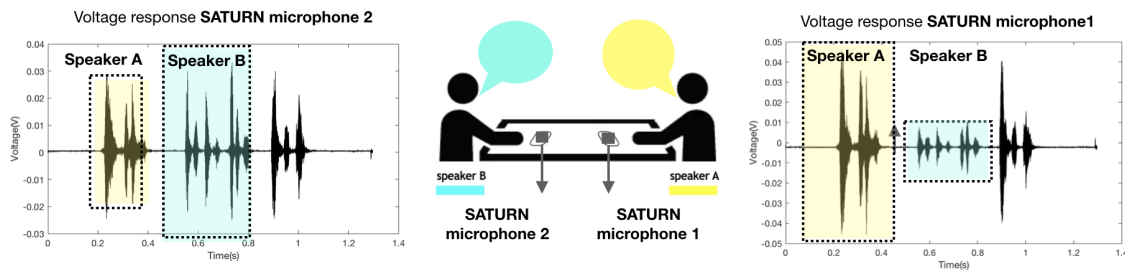


Fig. 26. Localization of speakers around a tabletop : Multiple SATURN microphones are placed on the table for localization of speaker. The SATURN microphone placed nearer to the the speaker has more voltage output e.g. the microphone 1 has higher electrical output than microphone 2 when speaker A speaks and vice versa

9.2 A Sound-sensitive Bottle

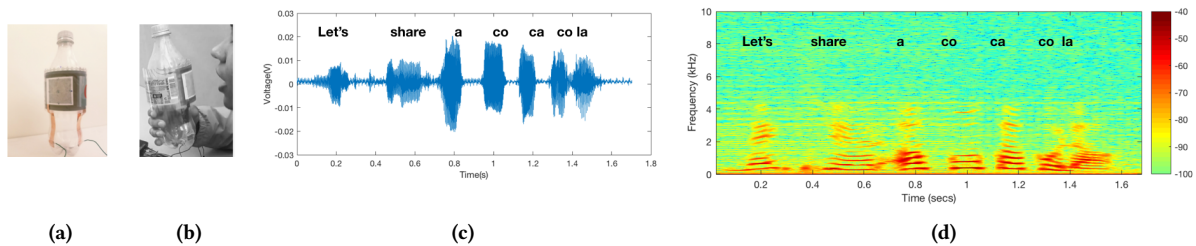


Fig. 27. A Sound-sensitive Bottle : (a) SATURN microphone embedded in a soda bottle (b) user talking to soda bottle (c) recovered audio signal (d) spectrogram

The SATURN microphone's flexibility and form factor allows the possibility of attaching a microphone to everyday objects, such as a bottle (Figure 27a). A $4 \times 4 \text{ cm}^2$ SATURN patch was placed on a soda bottle to enable interactions. A person may give voice commands like - "let's share a coca cola" which can enable control like actuating a display (Figure 27b). The time series graph of live speech is shown in the time series voltage (Figure 27c) with corresponding spectrogram (Figure 27d), which shows sufficient detail to do spectral feature extraction. With appropriate storage, computation and communication, we can imagine a wide variety of interactive voice-activated capabilities, and that is a direction we are pursuing.

9.3 Ambient Monitoring of Acoustic Scenes

In Section 8, we characterized the capabilities of SATURN as a power harvesting solution. Here, we demonstrate how that power can be used to flip a bit in a non-volatile memory cell in response to a loud sound. Next, we suggest how that bit might be read using a passive RFID mechanism. Such a system could be used for inexpensive, battery-free ambient monitoring of sources of noise pollution. Going further, we suggest that SATURN could power radio transmitters being designed in the literature [35, 61] as long as the sound was maintained, allowing real-time alerts to sounds that exceed a loudness threshold. In this manner, acoustic environmental monitoring can be performed without the cost and environmental difficulties of batteries.

Applications include monitoring for sound thresholds exceeding human hearing tolerance, such as in construction zones, mines, music venues, power stations, airports, spaceports, and military environments. Similarly, SATURN-based sensors might be used for monitoring events such as landslides, avalanches, polar ice breaking, mine cave-ins, and mine gas explosions. In a more futuristic application, United Nations could drop SATURN-based sensors from an airplane into a conflict zone. The sensors would monitor the acoustic environment for the movement of tanks, mortars, or exploding ordinance. Later, an officer with a reading device might sweep the field to interrogate the sensors. In a more extreme scenario, a low flying helicopter might sweep a strong RF signal over the region and record which sensors report hearing an event. The pattern of reporting sensors can reveal the direction of travel and point to possible hiding areas for that equipment which could possibly prevent destruction and loss of lives.

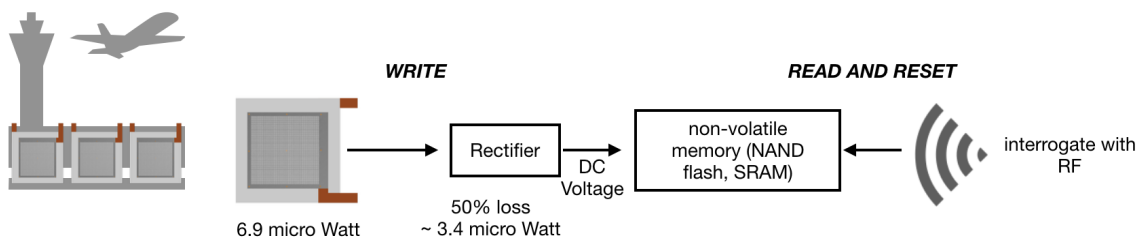


Fig. 28. Recording a loud acoustic event using power generated from a SATURN microphone.

As a motivating example, imagine an airport that would like to monitor its acoustic environment so as to not exceed safe noise levels for its employees or to keep aircraft noise footprints within airport boundaries as shown in Figure 28. A SATURN-based system can be tiled on various buildings and at various distances on the runway. As planes take off, they generate loud sounds due to gears, fans, and air turbulence. The peak in the sound spectrum generated by aircraft is near the 200-300 Hz band (Figure 45 in [21]) with decibel levels reaching $> 105 \text{ db}_{SPL}$ at 5 m^4 . These values are consistent with the resonant frequency of the SATURN patch and would result in generation of power $> 6.9 \mu\text{W}$ accumulated over different frequency bands. Considering the maximum power transfer theorem (Jacobi's law) the usable power we can obtain from such phenomenon is approximately

⁴NASA jet engine spectra : <https://www.grc.nasa.gov/WWW/Acoustics/Education/InternArchive/Schifer.htm>

50%. Thus, we might harvest up to $3.4 \mu\text{W}$. The energy required to program a “1” in a NAND flash memory is $2\mu\text{J}$ [37]. Given that the sounds we are expecting will probably last for several seconds, there is more than enough power to record the acoustic event. Going further, SRAM bits can be flipped at approximately 10-100 pW of power [14, 51], suggesting that rudimentary computation might be performed to determine if the flash memory bit should be written. A worker can then visit each SATURN site, interrogating the system using a passive RFID mechanism. When the worker places the active RFID reader above each SATURN system, it reads the state of the recorded bit and resets the system so that it is ready to catch the next episode.

Going further, after detecting a loud sound, the SATURN system might use its harvested power to power a RF transmitter to announce the event. For example, Talla et al. [60] have recently demonstrated an 915MHz analog LoRa backscatter communications device that can communicate at greater than 11 bits/sec while hundreds of meters away from its RF source and receiving antenna. While their system currently uses a battery, their theoretical IC design consumes only 9.25 micro-watts of power. With sound events lasting on the order of seconds, one can imagine a SATURN-based system storing power until it has enough to enable a 915Mhz backscatter transmission to the receiving antenna, announcing the event. As long as the event continues to occur, the SATURN system can transmit alerts every few seconds to a remote monitoring station.

For applications where the remote monitoring station can be closer, a SATURN-based system might transmit audio instead of simply an alert. Again, recent work by Talla et al. [61] has shown a “battery-free” phone which is powered by a transmitter 9.4 meters away. The system requires only 3.48 micro-watts of power to run continuously, which is barely within the range of what a SATURN patch might produce. Leveraging the implementation tested by these researchers, one can imagine a system design where SATURN provides both the power and the signal to stream audio during a loud acoustic event. More practically, however, SATURN might store power for a few seconds at the beginning of an event and then connect to the remote server to stream audio for a few seconds. In this manner the system might provide a further transmit distance.

10 DISCUSSION

10.1 Limitations of SATURN Microphone Design

We have discussed how SATURN microphone is a passive audio sensor that may enable systems to save power on the sensing layer of a low power infrastructure, and although SATURN still requires an external signal processing, we explored possibilities to leverage signal processing through low power analog wireless communication and computing.

As part of that goal, for this self-powered design we removed components that required external power to operate and are common in commercial microphones, such as amplifiers. This comes at the price of reduced audio sensitivity, and as a result the SATURN patch’s performance drops off at frequencies above 5kHz. Though we have only scratched the surface in terms of optimizing the design for performance, our implemented applications demonstrate there are already compelling uses for SATURN.

As a result of the design and the materials selected for fabrication, the SATURN patch may be affected by environmental conditions such as humidity, wind and extreme vibration. Most of the tests conducted were under controlled environments, and further analysis is required for determining the effect of such adversarial conditions, as well as overall durability of the design over time.

10.2 Future Work

We were able to improve the SATURN microphone design by introducing new structural parameters, specifically hole dimensions and attachment points in the paper layer. A more comprehensive model of the paper and PTFE layers and their interactions will provide deeper understanding into the attachment points for patches of different

sizes, shapes and flexibility. This could also help design SATURN microphone patches tuned at different resonant frequencies for different applications.

We have described a semi-automated manufacturing process for the SATURN microphone. There is great motivation to explore the automation of the production of SATURN-like microphones. In addition to a more exhaustive exploration of the design parameters of a single patch, there is an interesting opportunity to explore very large scale and coordinated SATURN patches that could cover a whole table surface or wall, resulting in a microphone array. We are investigating ways to connect SATURN patches via printed electronics and other low-cost scalable manufacturing techniques. Some applications of SATURN microphone patches suggest a disposable use, such as a label on a bottle. The low cost of SATURN makes that a possibility. Other applications, such as enabling a tabletop surface or wall to do auditory scene analysis or a building/road surface triggering noise alerts, consider the long-term use of such a material. The former short-term applications require very inexpensive manufacturing processes, while the latter require durability.

When we discussed the use of SATURN patches to perform ambient monitoring of acoustic scenes, we introduced the opportunity to transmit the harvested audio signal off the SATURN patch via mechanisms like analog backscatter [61]. This opens up the possibility of more self-sustained application scenarios, what we consider the most compelling direction for our future research. To take advantage of SATURN microphone as a self-powered sensor with high acoustic sensitivity, we should either connect it to low power processor [13, 49, 55] which allows for both operation and recognition of sound in about a few tens of micro-watts as shown in Figure 29 or send the audio to remote base station for recognition using analog backscatter [61] which would only consumes a few micro-watts which can be harvested from the environment.

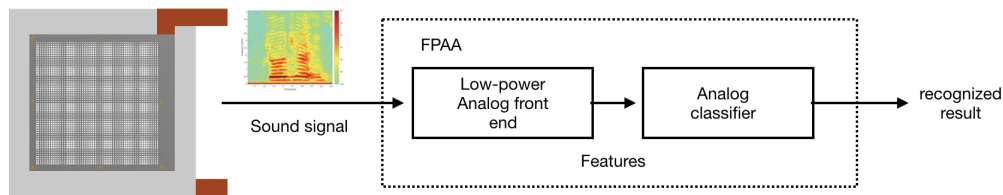


Fig. 29. Low-power realtime local sensing and recognition system design : Schematic diagram of self-powered analog sensor like SATURN microphone connected to analog recognition SoC like Field Programmable Analog Arrays[13]

11 CONCLUSION

Inspired by earlier work in materials science that demonstrated the opportunities for harvesting energy from the triboelectric effect, we have presented the design, evaluation and potential use of the SATURN microphone. The thin and flexible two-layer SATURN microphone design has favorable audio performance when compared to other passive and active microphones and requires no power. SATURN's simple fabrication process and ease of deployment on a variety of surfaces enables new opportunities for audio sensing over large indoor/outdoor areas for both mobile and stationary objects. SATURN may enable battery-less remote sensing for acoustic events, which has potential applications in controlling noise pollution, workplace safety, environmental monitoring, and military situation awareness.

ACKNOWLEDGMENTS

The authors would like to thank Dr. Byron Boots, Dr. Jennifer Hasler, Dr. Omer Inan, Dr. Cheng Zhang and Dr. Mark Clements for their discussions and feedback which help shape this work.

REFERENCES

- [1] Roberto Aimi. 2007. Percussion instruments using realtime convolution: Physical controllers. In *Proceedings of the 7th international conference on New interfaces for musical expression*. ACM, 154–159.
- [2] Thiago AL Burgo, Telma RD Ducati, Kelly R Francisco, Karl J Clinckspoor, Fernando Galembeck, and Sergio E Galembeck. 2012. Triboelectricity: macroscopic charge patterns formed by self-arraying ions on polymer surfaces. *Langmuir* 28, 19 (2012), 7407–7416.
- [3] Jun Chen, Guang Zhu, Weiqing Yang, Qingshen Jing, Peng Bai, Ya Yang, Te-Chien Hou, and Zhong Lin Wang. 2013. Harmonic-resonator-based triboelectric nanogenerator as a sustainable power source and a self-powered active vibration sensor. *Advanced materials* 25, 42 (2013), 6094–6099.
- [4] Tanzeem Choudhury and Alex Pentland. 2003. Sensing and modeling human networks using the sociometer. *IEEE*, 216.
- [5] Mary T Cord, Rauna K Surr, Brian E Walden, and Laurel Olson. 2002. Performance of directional microphone hearing aids in everyday life. *Journal of the American Academy of Audiology* 13, 6 (2002), 295–307.
- [6] Kai Dong, Jianan Deng, Yunlong Zi, Yi-Cheng Wang, Cheng Xu, Haiyang Zou, Wenbo Ding, Yejing Dai, Bohong Gu, Baozhong Sun, et al. 2017. 3D Orthogonal Woven Triboelectric Nanogenerator for Effective Biomechanical Energy Harvesting and as Self-Powered Active Motion Sensors. *Advanced Materials* 29, 38 (2017), 1702648.
- [7] John Eargle. 2012. *The Microphone Book: From mono to stereo to surround—a guide to microphone design and application*. CRC Press.
- [8] Gary W Elko and Kieran P Harney. 2009. A History of Consumer Microphones: The Electret Condenser Microphone Meets Micro-Electro-Mechanical-Systems. *Acoustics Today* 5, 2 (2009), 4–13.
- [9] Tiago H Falk, Chenxi Zheng, and Wai-Yip Chan. 2010. A non-intrusive quality and intelligibility measure of reverberant and dereverberated speech. *IEEE Transactions on Audio, Speech, and Language Processing* 18, 7 (2010), 1766–1774.
- [10] Xing Fan, Jun Chen, Jin Yang, Peng Bai, Zhaoling Li, and Zhong Lin Wang. 2015. Ultrathin, rollable, paper-based triboelectric nanogenerator for acoustic energy harvesting and self-powered sound recording. *ACS nano* 9, 4 (2015), 4236–4243.
- [11] Freeman W Fraim, Preston V Murphy, and Robert J Ferran. 1973. Electrets in miniature microphones. *The Journal of the Acoustical Society of America* 53, 6 (1973), 1601–1608.
- [12] J Frieden. 2005. Modern sensors. *Handbook. Moscow, Technosphere* (2005).
- [13] Suma George, Sihwan Kim, Sahil Shah, Jennifer Hasler, Michelle Collins, Farhan Adil, Richard Wunderlich, Stephen Nease, and Shubha Ramakrishnan. 2016. A programmable and configurable mixed-mode FPAA SoC. *IEEE Transactions on Very Large Scale Integration (VLSI) Systems* 24, 6 (2016), 2253–2261.
- [14] Nad Gilbert, Yanqing Zhang, John Dinh, Benton Calhoun, and Shane Hollmer. 2013. A 0.6 V 8 pJ/write non-volatile CBRAM macro embedded in a body sensor node for ultra low energy applications. In *VLSI Circuits (VLSIC), 2013 Symposium on*. IEEE, C204–C205.
- [15] Victor Giurgiutiu. 2007. *Structural health monitoring: with piezoelectric wafer active sensors*. Academic Press.
- [16] Ebenezer Hailemariam, Rhys Goldstein, Ramtin Attar, and Azam Khan. 2011. Real-time occupancy detection using decision trees with multiple sensor types. In *Proceedings of the 2011 Symposium on Simulation for Architecture and Urban Design*. Society for Computer Simulation International, 141–148.
- [17] Xu He, Yunlong Zi, Hua Yu, Steven L Zhang, Jie Wang, Wenbo Ding, Haiyang Zou, Wei Zhang, Canhui Lu, and Zhong Lin Wang. 2017. An ultrathin paper-based self-powered system for portable electronics and wireless human-machine interaction. *Nano Energy* 39 (2017), 328–336.
- [18] Invensense. 2014. Invensense INMP441. <https://www.invensense.com/products/digital/inmp441/>
- [19] Mustafa Emre Karagozler, Ivan Poupyrev, Gary K Fedder, and Yuri Suzuki. 2013. Paper generators: harvesting energy from touching, rubbing and sliding. In *Proceedings of the 26th annual ACM symposium on User interface software and technology*. ACM, 23–30.
- [20] Yoshihiro Kawahara, Steve Hodges, Benjamin S Cook, Cheng Zhang, and Gregory D Abowd. 2013. Instant inkjet circuits: lab-based inkjet printing to support rapid prototyping of UbiComp devices. In *Proceedings of the 2013 ACM international joint conference on Pervasive and ubiquitous computing*. ACM, 363–372.
- [21] Mehdi R Khorrami, Ehab Fares, and Damiano Casalino. 2014. Towards full aircraft airframe noise prediction: lattice Boltzmann simulations. In *20th AIAA/CEAS aeroacoustics conference*. 2481.
- [22] Sunkook Kim, Hyuk-Jun Kwon, Sunghun Lee, Hongshik Shim, Youngtea Chun, Woong Choi, Jinho Kwack, Dongwon Han, MyoungSeop Song, Sungchul Kim, et al. 2011. Low Power Flexible Organic Light-Emitting Diode Display Device. *Advanced Materials* 23, 31 (2011), 3511–3516.
- [23] Soo-Jin Kim and Jang-Sik Lee. 2010. Flexible organic transistor memory devices. *Nano letters* 10, 8 (2010), 2884–2890.
- [24] Sang Choon Ko, Yong Chul Kim, Seung Seob Lee, Seung Ho Choi, and Sang Ryong Kim. 2003. Micromachined piezoelectric membrane acoustic device. *Sensors and Actuators A: Physical* 103, 1 (2003), 130–134.
- [25] Timilehin Labeodan, Wim Zeiler, Gert Boxem, and Yang Zhao. 2015. Occupancy measurement in commercial office buildings for demand-driven control applications : A survey and detection system evaluation. *Energy and Buildings* 93 (2015), 303–314.
- [26] Oscar D Lara and Miguel A Labrador. 2013. A survey on human activity recognition using wearable sensors. *IEEE Communications Surveys and Tutorials* 15, 3 (2013), 1192–1209.

- [27] Eric C Larson, Mayank Goel, Gaetano Boriello, Sonya Heltshe, Margaret Rosenfeld, and Shwetak N Patel. 2012. SpiroSmart: using a microphone to measure lung function on a mobile phone. In *Proceedings of the 2012 ACM Conference on Ubiquitous Computing*. ACM, 280–289.
- [28] Jerad Lewis. 2012. Understanding microphone sensitivity. *Analog Dialogue* 46, 2 (2012), 14–16.
- [29] Jerad Lewis and Brian Moss. 2013. MEMS Microphone: The Future for Hearing Aids. *Analog Dialogue* 47 (2013), 3–5.
- [30] Bo Li, Tara Sainath, Arun Narayanan, Joe Caroselli, Michiel Bacchiani, Ananya Misra, Izhak Shafran, Hasim Sak, Golan Pundak, Kean Chin, et al. 2017. Acoustic Modeling for Google Home. (2017).
- [31] Wei Li, David Torres, Ramón Díaz, Zhengjun Wang, Changsheng Wu, Chuan Wang, Zhong Lin Wang, and Nelson Sepúlveda. 2017. Nanogenerator-based dual-functional and self-powered thin patch loudspeaker or microphone for flexible electronics. *Nature Communications* 8 (2017).
- [32] Long Lin, Sihong Wang, Simiao Niu, Chang Liu, Yinnan Xie, and Zhong Lin Wang. 2014. Noncontact free-rotating disk triboelectric nanogenerator as a sustainable energy harvester and self-powered mechanical sensor. *ACS applied materials & interfaces* 6, 4 (2014), 3031–3038.
- [33] Long Lin, Yinnan Xie, Sihong Wang, Wenzhuo Wu, Simiao Niu, Xiaonan Wen, and Zhong Lin Wang. 2013. Triboelectric active sensor array for self-powered static and dynamic pressure detection and tactile imaging. *ACS nano* 7, 9 (2013), 8266–8274.
- [34] Ruiyuan Liu, Xiao Kuang, Jianan Deng, Yi-Cheng Wang, Aurelia C Wang, Wenbo Ding, Ying-Chih Lai, Jun Chen, Peihong Wang, Zhiqun Lin, et al. 2018. Shape Memory Polymers for Body Motion Energy Harvesting and Self-Powered Mechanosensing. *Advanced Materials* (2018), 1705195. <https://doi.org/10.1002/adma.201705195>
- [35] Vincent Liu, Aaron Parks, Vamsi Talla, Shyamnath Gollakota, David Wetherall, and Joshua R Smith. 2013. Ambient backscatter: wireless communication out of thin air. In *ACM SIGCOMM Computer Communication Review*, Vol. 43. ACM, 39–50.
- [36] Gaurav Mathur, Peter Desnoyers, Paul Chukiu, Deepak Ganesan, and Prashant Shenoy. 2009. Ultra-low power data storage for sensor networks. *ACM Transactions on Sensor Networks (TOSN)* 5, 4 (2009), 33.
- [37] Vidyabhushan Mohan, Trevor Bunker, Laura Grupp, Sudhanva Gurumurthi, Mircea R Stan, and Steven Swanson. 2013. Modeling power consumption of nand flash memories using flashpower. *IEEE Transactions on Computer-Aided Design of Integrated Circuits and Systems* 32, 7 (2013), 1031–1044.
- [38] Kei Nakatsuma, Rhoma Takedomi, Takaaki Eguchi, Yasutaka Oshima, and Ippei Torigoe. 2015. Active bioacoustic measurement for human-to-human skin contact area detection. In *SENSORS, 2015 IEEE*. IEEE, 1–4.
- [39] Arokia Nathan, Arman Ahnood, Matthew T Cole, Sungsik Lee, Yuji Suzuki, Pritesh Hiralal, Francesco Bonaccorso, Tawfique Hasan, Luis Garcia-Gancedo, Andriy Dyadyusha, et al. 2012. Flexible electronics: the next ubiquitous platform. *Proc. IEEE* 100, Special Centennial Issue (2012), 1486–1517.
- [40] Jun Nishimura and Tadahiro Kuroda. 2008. Eating habits monitoring using wireless wearable in-ear microphone. In *Wireless Pervasive Computing, 2008. ISWPC 2008. 3rd International Symposium on*. IEEE, 130–132.
- [41] Simiao Niu, Sihong Wang, Long Lin, Ying Liu, Yu Sheng Zhou, Youfan Hu, and Zhong Lin Wang. 2013. Theoretical study of contact-mode triboelectric nanogenerators as an effective power source. *Energy & Environmental Science* 6, 12 (2013), 3576–3583.
- [42] Kenji Nomura, Hiromichi Ohta, Kazushige Ueda, Toshio Kamiya, Masahiro Hirano, and Hideo Hosono. 2003. Thin-film transistor fabricated in single-crystalline transparent oxide semiconductor. *Science* 300, 5623 (2003), 1269–1272.
- [43] Changhyun Pang, Chanseok Lee, and Kahp-Yang Suh. 2013. Recent advances in flexible sensors for wearable and implantable devices. *Journal of Applied Polymer Science* 130, 3 (2013), 1429–1441.
- [44] Joseph A. Paradiso. 1996. The interactive balloon: Sensing, actuation and behavior in a common object. *IBM Systems Journal* 35, 3.4 (1996), 473–487.
- [45] Shwetak N Patel and Gregory D Abowd. 2007. Blui: low-cost localized blowable user interfaces. In *Proceedings of the 20th annual ACM symposium on User interface software and technology*. ACM, 217–220.
- [46] Michael Pederson, Wouter Olthuis, and Piet Bergveld. 1998. High-performance condenser microphone with fully integrated CMOS amplifier and DC-DC voltage converter. *Journal of Microelectromechanical Systems* 7, 4 (1998), 387–394.
- [47] Massoud Pedram and Jan M Rabaey. 2002. *Power aware design methodologies*. Springer Science & Business Media.
- [48] Arthur N Popper, Richard R Fay, and Arthur N Popper. 2005. *Sound source localization*. Springer.
- [49] Michael Price, James Glass, and Anantha P Chandrakasan. 2017. A Low-Power Speech Recognizer and Voice Activity Detector Using Deep Neural Networks. *IEEE Journal of Solid-State Circuits* (2017).
- [50] Yi Qi and Michael C McAlpine. 2010. Nanotechnology-enabled flexible and biocompatible energy harvesting. *Energy & Environmental Science* 3, 9 (2010), 1275–1285.
- [51] P Raikwal, V Neema, and A Verma. 2017. High speed 8T SRAM cell design with improved read stability at 180nm technology. In *Electronics, Communication and Aerospace Technology (ICECA), 2017 International conference of*, Vol. 2. IEEE, 563–568.
- [52] Meital Segev-Bar and Hossam Haick. 2013. Flexible sensors based on nanoparticles. *ACS nano* 7, 10 (2013), 8366–8378.
- [53] Wan-Ho Seol, Yong Min Lee, and Jung-Ki Park. 2007. Enhancement of the mechanical properties of PVDF membranes by non-solvent aided morphology control. *Journal of Power Sources* 170, 1 (2007), 191–195.

- [54] GM Sessler and JE West. 1973. Electret transducers: a review. *The Journal of the Acoustical Society of America* 53, 6 (1973), 1589–1600.
- [55] Sahil Shah, Caitlin N Teague, Omer T Inan, and Jennifer Hasler. 2016. A proof-of-concept classifier for acoustic signals from the knee joint on a FPAA. In *SENSORS, 2016 IEEE*. IEEE, 1–3.
- [56] Richard C Simpson and Simon P Levine. 2002. Voice control of a powered wheelchair. *IEEE Transactions on Neural Systems and Rehabilitation Engineering* 10, 2 (2002), 122–125.
- [57] Sparkfun. 2000. Foil Electret microphone datasheet. <https://cdn.sparkfun.com/datasheets/Sensors/Sound/CEM-C9745JAD462P2.54R.pdf>
- [58] Sparkfun. 2012. SparkFun MEMS Microphone Breakout - INMP401 (ADMP401). <https://www.sparkfun.com/products/9868>
- [59] Thad Starner. 2001. The challenges of wearable computing: Part 1. *Ieee Micro* 21, 4 (2001), 44–52.
- [60] Vamsi Talla, Mehrdad Hesar, Bryce Kellogg, Ali Najafi, Joshua R Smith, and Shyamnath Gollakota. 2017. LoRa backscatter: Enabling the vision of ubiquitous connectivity. *Proceedings of the ACM on Interactive, Mobile, Wearable and Ubiquitous Technologies* 1, 3 (2017), 105.
- [61] Vamsi Talla, Bryce Kellogg, Shyamnath Gollakota, and Joshua R Smith. 2017. Battery-Free Cellphone. *Proceedings of the ACM on Interactive, Mobile, Wearable and Ubiquitous Technologies* 1, 2 (2017), 25.
- [62] J-M Valin, François Michaud, Jean Rouat, and Dominic Létourneau. 2003. Robust sound source localization using a microphone array on a mobile robot. In *Intelligent Robots and Systems, 2003.(IROS 2003). Proceedings. 2003 IEEE/RSJ International Conference on*, Vol. 2. IEEE, 1228–1233.
- [63] Tim Van Kasteren, Athanasios Noulas, Gwenn Englebienne, and Ben Kröse. 2008. Accurate activity recognition in a home setting. In *Proceedings of the 10th international conference on Ubiquitous computing*. ACM, 1–9.
- [64] Zhong Lin Wang. 2013. Triboelectric nanogenerators as new energy technology for self-powered systems and as active mechanical and chemical sensors. *ACS nano* 7, 11 (2013), 9533–9557.
- [65] Zhong Lin Wang. 2015. Triboelectric nanogenerators as new energy technology and self-powered sensors—Principles, problems and perspectives. *Faraday discussions* 176 (2015), 447–458.
- [66] Zhong Lin Wang. 2017. On Maxwell’s displacement current for energy and sensors: the origin of nanogenerators. *Materials Today* 20, 2 (2017), 74 – 82.
- [67] Zhong Lin Wang, Jun Chen, and Long Lin. 2015. Progress in triboelectric nanogenerators as a new energy technology and self-powered sensors. *Energy & Environmental Science* 8, 8 (2015), 2250–2282.
- [68] Zhong Lin Wang and Jinhui Song. 2006. Piezoelectric nanogenerators based on zinc oxide nanowire arrays. *Science* 312, 5771 (2006), 242–246.
- [69] Zhong Lin Wang and Aurelia Chi Wang. 2018. Triboelectric Nanogenerator for Self-Powered Flexible Electronics and Internet of Things. In *Meeting Abstracts*. The Electrochemical Society, 1533–1533.
- [70] Kajiro Watanabe, Yosuke Kurihara, Tetsuo Nakamura, and Hiroshi Tanaka. 2010. Design of a low-frequency microphone for mobile phones and its application to ubiquitous medical and healthcare monitoring. *IEEE Sensors Journal* 10, 5 (2010), 934–941.
- [71] JW Weigold, TJ Brosnihan, J Bergeron, and X Zhang. 2006. A MEMS condenser microphone for consumer applications. In *Micro Electro Mechanical Systems, 2006. MEMS 2006 Istanbul. 19th IEEE International Conference on*. IEEE, 86–89.
- [72] William S Wong and Alberto Salleo. 2009. *Flexible electronics: materials and applications*. Vol. 11. Springer Science & Business Media.
- [73] Minyi Xu, Peihong Wang, Yi-Cheng Wang, Steven L Zhang, Aurelia Chi Wang, Chunli Zhang, Zhengjun Wang, Xinxiang Pan, and Zhong Lin Wang. 2018. A Soft and Robust Spring Based Triboelectric Nanogenerator for Harvesting Arbitrary Directional Vibration Energy and Self-Powered Vibration Sensing. *Advanced Energy Materials* 8, 9 (2018), 1702432.
- [74] Minyi Xu, Yi-Cheng Wang, Steven L Zhang, Wenbo Ding, Jia Cheng, Xu He, Peng Zhang, Zhengjun Wang, Xinxiang Pan, and Zhong Lin Wang. 2017. An aeroelastic flutter based triboelectric nanogenerator as a self-powered active wind speed sensor in harsh environment. *Extreme Mechanics Letters* 15 (2017), 122–129.
- [75] Jin Yang, Jun Chen, Ying Liu, Weiqing Yang, Yuanjie Su, and Zhong Lin Wang. 2014. Triboelectrification-Based Organic Film Nanogenerator for Acoustic Energy Harvesting and Self-Powered Active Acoustic Sensing. *ACS Nano* 8, 3 (2014), 2649–2657.
- [76] Po-Kang Yang, Zong-Hong Lin, Ken C Pradel, Long Lin, Xiuhua Li, Xiaonan Wen, Jr-Hau He, and Zhong Lin Wang. 2015. paper-based origami triboelectric nanogenerators and self-powered pressure sensors. *ACS nano* 9, 1 (2015), 901–907.
- [77] Hulin Zhang, Ya Yang, Yuanjie Su, Jun Chen, Katherine Adams, Sangmin Lee, Chenguo Hu, and Zhong Lin Wang. 2014. Triboelectric nanogenerator for harvesting vibration energy in full space and as self-powered acceleration sensor. *Advanced Functional Materials* 24, 10 (2014), 1401–1407.
- [78] Steven L Zhang, Ying-Chih Lai, Xu He, Ruiyuan Liu, Yunlong Zi, and Zhong Lin Wang. 2017. Auxetic Foam-Based Contact-Mode Triboelectric Nanogenerator with Highly Sensitive Self-Powered Strain Sensing Capabilities to Monitor Human Body Movement. *Advanced Functional Materials* 27, 25 (2017).
- [79] Lisong Zhou, Alfred Wanga, Sheng-Chu Wu, Jie Sun, Sungkyu Park, and Thomas N Jackson. 2006. All-organic active matrix flexible display. *Applied Physics Letters* 88, 8 (2006), 083502.
- [80] Yaniv Zigel, Dima Litvak, and Israel Gannot. 2009. A method for automatic fall detection of elderly people using floor vibrations and sound : Proof of concept on human mimicking doll falls. *IEEE Transactions on Biomedical Engineering* 56, 12 (2009), 2858–2867.

Received November 2017; revised February 2018; accepted April 2018